

# Two-level Nonlinear Preconditioning Methods for Flood Models Posed on Perforated Domains

Miranda Boutilier<sup>a,\*</sup>, Konstantin Brenner<sup>a,b</sup>, Victorita Dolean<sup>c</sup>

<sup>a</sup>*Université Côte d'Azur, Laboratoire J.A. Dieudonné, CNRS UMR 7351, Nice, 06108, France*

<sup>b</sup>*Team COFFEE, INRIA Centre at Université Côte d'Azur, Nice, 06108, France*

<sup>c</sup>*Eindhoven University of Technology, Department of Mathematics and Computer Science, Eindhoven, 5600 MB, The Netherlands*

---

## Abstract

This article focuses on the numerical solution of the Diffusive Wave equation posed in a domain containing a large number of polygonal perforations. These numerous perforations represent structures in urban areas and this model problem is used to model urban floods. This article relies on the work done in a previous article by the same authors, in which we introduced low-dimensional coarse approximation space for the linear Poisson equation based on a coarse polygonal partitioning of the domain. Similarly to other multi-scale numerical methods, this coarse space is spanned by locally discrete harmonic basis functions. We show that this coarse space also lends itself to the linearized diffusive wave problem that is obtained at each iteration of Newton's method. Furthermore, we present nonlinear preconditioning techniques, including a two-level RASPEN and Two-step method, which can significantly reduce the number of iterations compared to the traditional Newton's method. Numerical examples illustrating the performance of the proposed methods include a large-scale test case based on topographical data from the city of Nice.

---

## 1. Introduction

In this article, we apply domain decomposition and multi-scale approaches to solve non-linear equations, both stationary and time-dependent. The main focus of the paper is the Diffusive Wave model [2], given by

$$\partial_t u - \operatorname{div} (c_f h(u, z_b(\mathbf{x}))^\alpha \|\nabla u\|^{\gamma-1} \nabla u) = f,$$

where  $z_b(\mathbf{x})$  represents bathymetry/topography,  $u$  is total water level,  $h(u, z_b(\mathbf{x})) = \max(u - z_b(\mathbf{x}, 0), 0)$  is the depth of the water with respect to bathymetry,  $c_f$  denotes friction,  $\gamma \leq 1$ , and  $1 \leq \alpha \leq 2$ . Generally, we take the source term  $f$  as constant; this source term can be considered to represent rainfall. The Diffusive Wave Equation (DWE) is doubly nonlinear

---

\*Corresponding Author

Email addresses: [miranda.boutilier@univ-cotedazur.fr](mailto:miranda.boutilier@univ-cotedazur.fr) (Miranda Boutilier),  
[konstantin.brenner@univ-cotedazur.fr](mailto:konstantin.brenner@univ-cotedazur.fr) (Konstantin Brenner), [v.dolean.maini@tue.nl](mailto:v.dolean.maini@tue.nl) (Victorita Dolean)

in the sense that there are nonlinearities both in the  $(u - z)$  term and in the gradient term. Additionally, the equation becomes degenerate, as  $\kappa(u, \nabla u) \rightarrow 0$  as  $h \rightarrow 0$  and  $\kappa(u, \nabla u) \rightarrow \infty$  as  $\nabla u \rightarrow 0$ . We can think of the DWE as a simplification of the 2D Shallow Water Equations with zero-inertia assumptions ; for this reason, the DWE is often referred to as the Zero Inertia (ZI) equations [2]. This equation is commonly used to model overland flows.

With this model problem, we wish to model overland flows in urban areas, particularly the area of Nice, France. Anticipating these flood events can aid in the positioning of protective systems including dams, dikes, or rainwater drainage networks. One of the challenges of this numerical modeling of urban floods is that small structural features (buildings, walls, etc.) may significantly affect the water flow. In particular, the representation of the structural features in the numerical model impacts both the timing and extent of the flood [30, 31, 1]. The data set used in this article has been provided by Métropole Nice Côte d’Azur (MNCA) and allows for an infra-metric description of the urban geometries [3]. From the hydraulic perspective, these structural features can be assumed to be essentially impervious, and therefore represented as perforations (holes) in the model domain.

With this, let  $D$  be an open simply connected polygonal domain in  $\mathbb{R}^2$ . We denote by  $(\Omega_{S,k})_k$  a finite family of perforations in  $D$  such that each  $\Omega_{S,k}$  is an open connected polygonal subdomain of  $D$ . The perforations are mutually disjoint, that is  $\overline{\Omega_{S,k}} \cap \overline{\Omega_{S,l}} = \emptyset$  for any  $k \neq l$ . We denote  $\Omega_S = \bigcup_k \Omega_{S,k}$  and  $\Omega = D \setminus \overline{\Omega_S}$ , assuming that the family  $(\Omega_{S,k})_k$  is such that  $\Omega$  is connected. The model problem of focus is given by the following: for a fixed time interval  $(0, T]$ ,

$$\begin{cases} \partial_t u - \operatorname{div}(\kappa(u, \nabla u) \nabla u) = 0 & \text{in } \Omega \times (0, T], \\ u = g & \text{on } (\partial\Omega \setminus \partial\Omega_S) \times (0, T], \\ \kappa(u, \nabla u) \frac{\partial u}{\partial \mathbf{n}} = 0 & \text{on } (\partial\Omega \cap \partial\Omega_S) \times (0, T], \end{cases} \quad (1)$$

where  $\mathbf{n}$  is the outward normal to the boundary,  $\kappa(u, \nabla u) = h(u, z_b(\mathbf{x}))^\alpha \|\nabla u\|^{\gamma-1}$ . The problem (1) must be combined with some initial condition on  $u$  such that  $u = u_0$  in  $\Omega \times (t = 0)$ .

In the context of urban flood modeling,  $(\Omega_{S,k})_k$  can be thought of as a family of impervious structures such as buildings, fences, or other similar structures. However, problems posed on perforated domains also arise in multiple real-world scenarios, such as fluid/groundwater flow in porous media, atmospheric models, battery models, and drug delivery systems. After some discretization to be detailed later, this nonlinear equation can be written as the nonlinear system

$$F(\mathbf{u}) = 0,$$

where the numerical solution  $\mathbf{u}$  approximates the exact solution  $u$ .

Depending on the geometrical complexity of the computational domain, the numerical solution of the PDE may become increasingly challenging. Our goal is to numerically solve the model problem on these perforated domains by using domain decomposition techniques. The latter use a divide and conquer approach to partition the domain into multiple smaller subdomains. Therefore, one has two “levels” of space discretization; the first level is based on a coarse polygonal partitioning of  $\Omega$ , while the second one is associated with the fine-scale triangulation and is designed to resolve the small-scale details of the model domain. The fine-scale triangulation is generated by Triangle [27]. Domain decomposition (DD) approaches to

solve nonlinear PDEs can generally split into two categories: Newton-Krylov Schwarz (NKS) and Schwarz Newton-Krylov (SNK) methods.

In NKS methods [6], the problem is first linearized, typically by Newton’s method or an inexact Newton method, which solve a linear system at each iteration. It is well-known that for large/complex linear systems, a direct linear solve can become quite expensive and time-consuming. In this case, one can then apply typical linear DD methods to this linear Newton system; i.e., use standard domain decomposition preconditioners coupled to a Krylov on the linear system to be solved at each Newton iteration. Therefore, in the case of NKS methods applied to a nonlinear problem  $F(\mathbf{u}) = 0$ , the system remains unchanged, and we use DD methods to make the linear solve more efficient.

Stiff nonlinearities arise in many nonlinear problems, including problems heterogeneous problems with high-contrast coefficients. These stiff nonlinearities can cause a plateau in the norm of the Newton residual before/if the quadratic region of convergence is reached. In these cases in a global Newton’s method, one may be forced to take very small time steps, or damp the Newton iteration to an extremely small damping factor. To combat this, more recently, SNK methods were introduced; these methods do not begin with a linearization and are commonly referred to as nonlinear preconditioning methods. In SNK methods, the nonlinear system itself is changed, unlike in NKS methods. The nonlinear preconditioners involve the solution of local nonlinear problems and can therefore localize stiff nonlinearities.

Specifically, given a nonlinear system  $F(\mathbf{u}) = 0$ , these SNK preconditioning methods solve a new nonlinear system  $\mathcal{F}(\mathbf{u})$  via Newton’s or inexact Newton’s method, where if  $\mathcal{F}(\mathbf{u}) = 0$ , then  $F(\mathbf{u}) = 0$  (i.e. the new nonlinear system shares solutions with the original nonlinear system). This system  $\mathcal{F}(\mathbf{u}) = 0$  is referred to as *the nonlinearly preconditioned system*. The latter is generated by applying Newton’s or inexact Newton’s method to a fixed point equation. The goal is for the nonlinearly preconditioned system to be solved faster than the original one; that is, to more quickly advance to the region of quadratic convergence for Newton’s method and reduce the number of exact or inexact Newton iterations.

In the Additive Schwarz Preconditioned Inexact Newton (ASPIN) [7], the authors introduce a method, where the nonlinearly preconditioned system  $\mathcal{F}(u) = 0$  consists of more balanced/uniform nonlinearities. ASPIN involves the solution of local nonlinear problems, using similar restriction and extension operators that are used in the linear case. Then, a global linear problem is solved via inexact Newton. In theory, for difficult problems with intense nonlinearities, this technique can accelerate convergence when compared to a typical Newton or inexact Newton method. Additionally, it can aid in the occurrence of stagnation in Newton’s method and desensitize Newton to the initial guess. We remark as well the existence of the MSPIN method [24], where generally, the partitioning of degrees of freedom is based on field type (field-splitting) instead of the typical subdomain partitioning. A main difference between the methods is that MSPIN can be thought of as analogous to the Multiplicative Schwarz (MS) method for linear systems, a generally non-parallel method, while ASPIN is analogous to the Additive Schwarz method (ASM). With this, one can also think of ASPIN and MSPIN as varying from each other in a similar manner to Jacobi and Gauss-Seidel methods. In MSPIN and ASPIN, inexact Newton solves are computed for the nonlinearly preconditioned system.

The authors of [13] extended the ASPIN method to form Restricted Additive Schwarz Preconditioned Exact Newton (RASPEN), which can be thought of as analogous to the linear RAS method. Similarly to the linear case, RASPEN does not sum contributions in the overlap, using partition of unity operators to form a fixed point iteration to which Newton’s method can be applied. The authors of [13] showed that by design, the nonlinearly preconditioned system  $\mathcal{F}_{RASPEN}(\mathbf{u}) = 0$  can be solved via exact Newton, as an equation can be derived for the exact Jacobian matrix  $\nabla \mathcal{F}_{RASPEN}(\mathbf{u})$ .

The authors of [10] introduced SRASPEN, which is obtained in a similar way by applying Newton’s method to the fixed point equation resulting from the nonlinear SRAS (Substructured Restricted Additive Schwarz) method. Unlike the aforementioned methods, the SRASPEN method works on nonoverlapping subdomains; these nonoverlapping domain decomposition methods are often referred to as substructuring methods. Within the same spirit, the authors of [11] introduced DNPEN, a nonlinear preconditioning method which applies Newton’s method to the Dirichlet-Neumann (DN) method, which is a substructuring method based on matching fluxes along subdomain interfaces. Additionally, the authors of [25] propose an adaptive nonlinear preconditioning technique which “turns off” the nonlinear preconditioning for outer Newtons where it is not necessary.

The aforementioned techniques can be considered as being *left preconditioning methods*, as they are solving a new tangential system  $\mathcal{F}(\mathbf{u}) = 0$  by exact or inexact Newton. We also remark that there are a family of *right nonlinear preconditioning techniques*; these methods change the unknowns of the original system. We can give as an example the following works [20, 26, 21, 22, 23], where the authors introduced nonlinear preconditioners analogous to the Finite Element Tearing and Interconnecting (FETI), Finite Element Tearing and Interconnecting Dual-Primal (FETI-DP), and Balancing Domain Decomposition by Constraints (BDDC) methods. Additionally, the authors of [8] introduced the Nonlinear Elimination Preconditioned Inexact Newton (NEPIN), where “problem” components of the residual are implicitly eliminated and a resulting modified Newton direction is computed. However, the focus of this article is *left nonlinear preconditioning techniques based on overlapping subdomains*.

As is the case for linear DD methods, two-level methods (methods which include a coarse correction/level), are often needed for scalability in nonlinear preconditioning methods. Particularly, the number of GMRES iterations for the global tangential solve will not be scalable without a coarse correction. The coarse component allows for global communication across all subdomains. In the original article introducing RASPEN [13], the authors proposed a Full Approximation Scheme (FAS) to apply the coarse level. For MSPIN, a multiplicative coarse correction counterpart was introduced. In [17], the author propose a linear coarse level for ASPIN and in [15], the authors provide numerical evidence of scalability of two-level variants of ASPIN and RASPEN. In particular, they propose multiple approaches of adding the coarse space correction (both additively and multiplicatively) based on Galerkin projections, and a numerical comparison of the methods is reported for different types of coarse spaces.

In this paper, we rely on the work done in [4], in which we introduced an MsFEM coarse space for the linear Poisson problem posed on the perforated domains. Here, for nonlinear problems, we focus on *left nonlinear preconditioning based on overlapping subdomains*, coupled

to techniques that use the coarse space proposed in [4] to provide scalability. We propose this linear coarse space as a component of a two-level Restricted Additive Schwarz preconditioner for a linearized Newton system which arises from the linearization of a nonlinear equation. Additionally, we use this coarse space as a component for multiple nonlinear methods including a two-level RASPEN method and a “Two-step” method originally introduced in [9] under the name NKS-RAS. While the coarse space of [4] was originally created based on the linear Poisson equation, we find that it is a fitting coarse space for nonlinear problems as well, and we use this in the later-mentioned two-level nonlinear preconditioning methods. For these nonlinear methods applied to a time-dependent problem, we implement an adaptive local time-stepping method which allows us to avoid a global time step reduction. In addition, this article serves as a numerical application of nonlinear preconditioning methods applied to nonlinear problems, containing multiple numerical examples with the main example being the doubly nonlinear Diffusive Wave model posed on complex domains containing multiple perforations. For all proposed methods, we provide the detailed complexities/costs of each iteration.

The remainder of the paper is structured as follows. Section 2 provides a detailed description of the finite-element/ finite-volume hybrid discretization used for the Diffusive Wave Equation. Section 3 describes the coarse space from [4], which will be used in the two-level methods described in the article. Section 4 summarizes domain decomposition methods for linear problems, presenting the well-known linear Additive Schwarz and Restricted Additive Schwarz methods. Section 5 describes the proposed methods in detail, followed by Section 5.1 which discusses the cost/complexity of the proposed algorithms. Section 6 provides numerical results, with experiments based on a porous media equation posed on both an L-shaped domain and a large urban domain, followed by the Diffusive Wave equation posed on a large urban domain. Section 7 concludes with a summary and description of future work.

## 2. 2D spatial discretization of Diffusive Wave equation

We now proceed with a discretization of the Diffusive Wave model (1). Let  $T_f > 0$  be the final flow simulation time and let  $0 = t_0 < t_1 < \dots < t_N = T_f$  be a family of real numbers such that  $\Delta t_n = t_{n+1} - t_n$ .

We consider the following semi-implicit time discretization of (1): for  $u^{n+1} = u|_{t_{n+1}}$ ,

$$\left\{ \begin{array}{lll} \frac{u^{n+1} - u^n}{\Delta t_n} - \operatorname{div} (c_f \kappa(u^{n+1}, \nabla u^n) \nabla u^{n+1}) & = & 0 \quad \text{in } \Omega, \\ u^{n+1} & = & g \quad \text{on } \partial\Omega \setminus \partial\Omega_S, \\ c_f \kappa(u^{n+1}, \nabla u^n) \frac{\partial u^{n+1}}{\partial \mathbf{n}} & = & 0 \quad \text{on } \partial\Omega \cap \partial\Omega_S, \end{array} \right. \quad (2)$$

where  $u^0$  is a provided initial condition.

Let  $\mathcal{T}$  denote the triangulation of  $\Omega$  which is conforming with respect to the partitioning  $(\Omega_j)_{j=1}^N$ . We introduce the finite element space defined by

$$V_h = \{v \mid v \in C^0(\overline{\Omega}), \quad \text{s.t.} \quad v|_t \in \mathbb{P}_1, \quad \text{for all } t \in \mathcal{T}\}.$$

Recalling the definition of the space  $H_{\partial\Omega \setminus \partial\Omega_S}^1(\Omega)$  defined in (7), let  $V_{h,0} = V_h \cap H_{\partial\Omega \setminus \partial\Omega_S}^1(\Omega)$  and let  $g_h \in V_h$  be some approximation of the boundary data  $g$ . The finite element discretization of (2) reads as: Find  $u_h^{n+1} \in V_h$  satisfying  $u_h^{n+1}|_{\partial\Omega \setminus \Omega_S} = g_h$  such that

$$\frac{1}{\Delta t_n} \int_{\Omega} (u_h^{n+1} - u_h^n) v_h \, d\mathbf{x} + \int_{\Omega} c_f \kappa(u_h^{n+1}, \nabla u_h^n) \nabla u_h^{n+1} \cdot \nabla v_h \, d\mathbf{x} = 0 \quad \text{for all } v_h \in V_{h,0}. \quad (3)$$

Let  $(\mathbf{x}_i)_{i=1}^{N_{\Omega}}$  denote the set of triangulation points; the set of point indices  $\{1, 2, \dots, N_{\Omega}\}$  is denoted by  $\mathcal{N}$ . We denote the nodal ‘‘hat’’ basis functions  $(\eta^\ell)_{\ell=1}^{N_{\Omega}}$ . Furthermore, we define  $u_i^{n+1}$  and  $u_\ell^{n+1}$  as the nodal values of the discrete solution at nodes  $\mathbf{x}_i$  and  $\mathbf{x}_\ell$  at  $t_{n+1}$ , respectively. Additionally, we set  $\mathcal{N}_T = \{i \in \mathcal{N} \mid \mathbf{x}_i \in \bar{T}\}$  for any triangle  $T \in \mathcal{T}$  ( $T$  assumed to be open) and denote  $\mathcal{T}_i$  as the subset of triangles connected to node  $i$  such that  $\mathcal{T}_i = \{T \in \mathcal{T} \mid \mathbf{x}_i \in \bar{T}\}$ . Furthermore, we denote by  $\mathcal{N}_i$  the set of nodes adjacent to node  $i$  such that  $\mathcal{N}_i = \bigcup_{T \in \mathcal{T}_i} \mathcal{N}_T$ . Finally, let  $\mathcal{N}_D$  denote the set of Dirichlet nodes such that  $\mathcal{N}_D = \{i \in \mathcal{N} \mid \mathbf{x}_i \in \partial\Omega \setminus \Omega_S\}$ .

In order to enhance the stability of the numerical scheme, we modify the finite element scheme by means of discretization techniques from finite volume methods. In particular, we introduce mass lumping in the accumulation and upwinding in diffusion term. This discretization technique is generally referred to as a Finite Volume- Finite Element (FV-FE) discretization [12], or it is often referred to as a Control Volume Finite Element method.

**Diffusion term:** Since  $\sum_{\ell \in \mathcal{N}_T} \nabla \eta_\ell = 0$  on each triangle  $T$ , we observe for the diffusive term that for  $i \in \mathcal{N}$ ,

$$\begin{aligned} \int_{\Omega} c_f \kappa(u_h^{n+1}, \nabla u_h^n) \nabla u_h^{n+1} \cdot \nabla \eta_i \, d\mathbf{x} &= \sum_{T \in \mathcal{T}_i} \sum_{\ell \in \mathcal{N}_T} c_f u_\ell^{n+1} \int_T \kappa(u_h^{n+1}, \nabla u_h^n) \nabla \eta_\ell \cdot \nabla \eta_i \, d\mathbf{x}, \\ &= \sum_{\ell \in \mathcal{N}_i} c_f (u_\ell^{n+1} - u_i^{n+1}) \sum_{T \in \mathcal{T}} \int_T \kappa(u_h^{n+1}, \nabla u_h^n) \nabla \eta_\ell \cdot \nabla \eta_i \, d\mathbf{x}, \\ &= \sum_{\ell \in \mathcal{N}_i} c_f (u_\ell^{n+1} - u_i^{n+1}) \sum_{T \in \mathcal{T}_i \cap \mathcal{T}_\ell} \int_T \kappa(u_h^{n+1}, \nabla u_h^n) \nabla \eta_\ell \cdot \nabla \eta_i \, d\mathbf{x}, \end{aligned}$$

In order to deal with the degeneracy of  $\kappa(u, \boldsymbol{\xi}) = h(u, z_b)^\alpha \|\boldsymbol{\xi}\|^{\gamma-1}$  for  $h(u, z_b) = 0$ , we introduce upwinding in our discretization. Denoting

$$\tau_{i\ell,T}^n = -c_f \left| \nabla u_h^n|_T \right|^{1-\gamma} \int_T \nabla \eta_\ell \cdot \nabla \eta_i \, d\mathbf{x} \quad \text{and} \quad \tau_{i\ell}^n = \sum_{T \in \mathcal{T}_i \cap \mathcal{T}_\ell} \tau_{i\ell,T}^n,$$

we introduce upstream water depth defined by

$$h_{i\ell}^{n+1} = \begin{cases} h(u_i^{n+1}, z_b(\mathbf{x}_i)) & \text{if } \tau_{i\ell}^n (u_i^{n+1} - u_\ell^{n+1}) \geq 0, \\ h(u_\ell^{n+1}, z_b(\mathbf{x}_\ell)) & \text{otherwise.} \end{cases}$$

Then, we approximate

$$\int_{\Omega} c_f \kappa(u_h^{n+1}, \nabla u_h^n) \nabla u_h^{n+1} \cdot \nabla \eta_i \, d\mathbf{x} \approx \sum_{\ell \in \mathcal{N}_i} \tau_{i\ell}^n (h_{i\ell}^{n+1})^\alpha (u_i^{n+1} - u_\ell^{n+1}) \quad \text{for all } i \in \mathcal{N} \setminus \mathcal{N}_D.$$

**Accumulation term:** Let  $M_{i\ell}$  denote the  $(i, \ell)$ th entry of a classical finite element matrix, that is  $M_{i\ell} = \int_{\Omega} \eta_i \eta_{\ell} \, d\mathbf{x}$ . Then, denoting  $m_i = \sum_{\ell=1}^{N_{\Omega}} M_{i\ell}$ , we approximate

$$\frac{1}{\Delta t_n} \int_{\Omega} (u_h^{n+1} - u_h^n) \cdot \eta_i \, d\mathbf{x} \approx \frac{m_i}{\Delta t_n} (u_i^{n+1} - u_i^n) \quad \text{for all } i \in \mathcal{N} \setminus \mathcal{N}_D.$$

The resulting combined FV-FE scheme writes as

$$\begin{cases} \frac{m_i}{\Delta t_n} (u_i^{n+1} - u_i^n) + \sum_{\ell \in \mathcal{N}_i} \tau_{i\ell}^n (h_{i\ell}^{n+1})^{\alpha} (u_i^{n+1} - u_{\ell}^{n+1}) = 0 & \text{for } i \in \mathcal{N} \setminus \mathcal{N}_D, \\ u_i^{n+1} = g_h(\mathbf{x}_i), & \text{for } i \in \mathcal{N}_D. \end{cases} \quad (4)$$

In matrix-vector notations for a given vector  $\mathbf{u} = (u_i)_{i \in \mathcal{N} \setminus \mathcal{N}_D}$ , the scheme can be summarized as follows: for time step  $n = 0, 1, \dots$ , solve

$$F(\mathbf{u}^{n+1}) = 0,$$

where the  $i$ th component of  $F(\mathbf{u}^{n+1})$  is given by

$$F(\mathbf{u}^{n+1})_i = \frac{m_i}{\Delta t_n} (u_i^{n+1} - u_i^n) + \sum_{\ell \in \mathcal{N}_i} \tau_{i\ell}^n (h_{i\ell}^{n+1})^{\alpha} (u_i^{n+1} - u_{\ell}^{n+1}) \quad \text{for } i \in \mathcal{N} \setminus \mathcal{N}_D, \quad (5)$$

and  $u_i^{n+1} = g_h(\mathbf{x}_i)$  for  $i \in \mathcal{N}_D$ .

### 3. Multiscale Coarse space

We now briefly describe the coarse space that will be used for all introduced two-level algorithms; we refer the reader to [4] for a detailed description. The coarse space is of the multiscale type, composed of piecewise harmonic basis functions with respect to a polygonal partitioning of the domain. The latter are computed via the numerical solutions of linear Laplace problems.

Consider a finite nonoverlapping polygonal partitioning of  $D$  denoted by  $(D_j)_{j=1, \dots, N}$  and an induced nonoverlapping partitioning of  $\Omega$  denoted by  $(\Omega_j)_{j=1, \dots, N}$  such that  $\Omega_j = D_j \cap \Omega$ . We will refer to  $(\Omega_j)_{j=1, \dots, N}$  as the coarse mesh over  $\Omega$ . Additionally, we denote by  $\Gamma$  its skeleton, that is  $\Gamma = \bigcup_{j=1, \dots, N} \partial\Omega_j \setminus \partial\Omega_S$ . Let  $(e_k)_{k=1, \dots, N_e}$  denote a nonoverlapping partitioning of the  $\Gamma$  such that each “coarse edge”  $e_k$  is an open planar segment, and we denote  $H = \max_{k=1, \dots, N_e} |e_k|$ . The set of coarse grid nodes is given by  $\mathcal{V} = \bigcup_{k=1, \dots, N_e} \partial e_k$ . Figure 1 illustrates the location of the coarse grid nodes that typically result from clipping  $(D_j)_j$  with  $\Omega_S$ .

Let  $H_{\Delta}^1(\Omega)$  be a subspace of  $H^1(\Omega)$  composed of piece-wise harmonic functions, weakly satisfying the homogeneous Neumann boundary conditions on  $\partial\Omega \cap \partial\Omega_S$ , that is

$$H_{\Delta}^1(\Omega) = \{ u \in H^1(\Omega) \mid (u|_{\Omega_j}, v)_{H^1(\Omega_j)} = 0 \quad \text{for all } v \in H_{\partial\Omega \setminus \partial\Omega_S}^1(\Omega_j) \}, \quad (6)$$

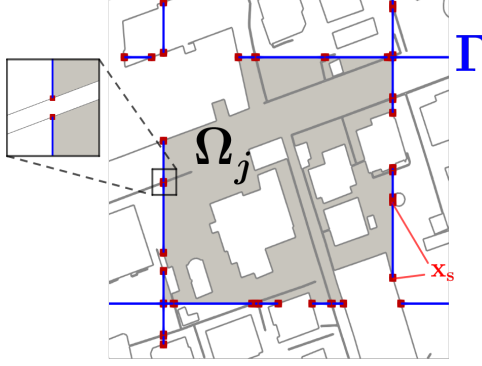


Figure 1: Coarse cell  $\Omega_j$ , nonoverlapping skeleton  $\Gamma$  (blue lines), and coarse grid nodes  $\mathbf{x}_s \in \mathcal{V}$  (red dots). Coarse grid nodes are located at  $\bar{\Gamma} \cap \partial\Omega_S$ .

where

$$H_{\partial\Omega \setminus \partial\Omega_S}^1(\Omega) = \{u \in H^1(\Omega) \mid u|_{\partial\Omega \setminus \partial\Omega_S} = 0\}. \quad (7)$$

In other words,  $u \in H_{\Delta}^1(\Omega)$  if and only if  $u \in H^1(\Omega)$  and for all subdomains  $\Omega_j$ , the equations

$$\begin{cases} -\Delta u|_{\Omega_j} = 0 & \text{in } \Omega_j, \\ \frac{\partial u}{\partial \mathbf{n}} = 0 & \text{on } \partial\Omega_j \cap \partial\Omega_S, \end{cases} \quad (8)$$

are satisfied in a weak sense.

With this, we define

$$V_H^\Gamma = \{v \in C^0(\bar{\Gamma}) \mid v|_{e_k} \in \mathbb{P}_1(e_k) \text{ for all } k = 1, \dots, N_e\},$$

where  $\mathbb{P}_1(e_k)$  denotes the set of piecewise linear polynomials over an edge  $e$ . We also define

$$V_H = \{v \in H_{\Delta}^1(\Omega) \mid v|_{\Gamma} \in V_H^\Gamma\},$$

where

Let  $(g_s)_{s=1, \dots, N_{\mathcal{V}}}$  be the nodal basis of  $V_H^\Gamma$ , where  $N_{\mathcal{V}}$  denotes the total number of coarse grid nodes. In practice,  $(g_s)_{s=1, \dots, N_{\mathcal{V}}}$  is composed of nodal piecewise linear “hat” functions. The function  $\phi_s \in V_H$  associated to  $g_s$  is computed by weakly imposing on each  $\Omega_j$

$$\begin{cases} \Delta \phi_s = 0 & \text{in } \Omega_j, \\ \frac{\partial \phi_s}{\partial \mathbf{n}} = 0 & \text{on } \partial\Omega_j \cap \partial\Omega_S, \\ \phi_s = g_s & \text{on } \partial\Omega_j \setminus \partial\Omega_S. \end{cases} \quad (9)$$

We refer to the space  $V_H$  as the Trefftz space. The basis of the discrete version of the Trefftz space is obtained through the finite element approximation of (9) which results in the system of the form

$$\tilde{A}_j \phi_s^j = b_s^j,$$



where  $\tilde{A}_j$  is the local stiffness matrix and  $b_s^j$  accounts for the Dirichlet boundary data in (9).

Let  $\bar{R}_j$  denote the boolean restriction matrices which restrict from the degrees of freedom in the discretization of  $\Omega$  to the degrees of freedom in the nonoverlapping subdomain  $\bar{\Omega}_j$ , and let  $\bar{D}_j$  denote partition of unity matrices corresponding to the discretization of  $\bar{\Omega}_j$  such that  $\sum_{j=1}^N \bar{R}_j^T \bar{D}_j R_j = I$ . Furthermore, let  $\phi_s$  be a global vector which, when restricted to a subdomain  $\Omega_j$ , returns  $\phi_s^j$ . That is,

$$\phi_s = \sum_{j \in \mathcal{N}_s} \bar{R}_j^T \bar{D}_j \phi_s^j,$$

for  $s = 1, \dots, N_V$ , where  $\mathcal{N}_s = \{j \mid \mathbf{x}_s \text{ is contained in } \Omega_j\}$ . The global vectors  $\phi_s$  are the basis vectors associated to the coarse grid nodes  $\mathbf{x}_s \in \mathcal{V}$ . The discrete Trefftz space is then defined as the span of the basis vectors  $\phi_s, s = 1, \dots, N_V$ . With this, the coarse transition matrix  $R_H$  is such that the  $k$ th row of  $R_H$  is given by  $\phi_k^T$  for  $k = 1, \dots, N_V$ .

#### 4. Linear Multi-domain Solution Methods

In this section, we summarize linear DD methods, particularly overlapping Schwarz methods, that will be extended in the next section to nonlinear PDEs. Consider some discretized linear system of the form

$$A\mathbf{u} = \mathbf{f}.$$

Let  $(\Omega'_j)_{j=1, \dots, N}$  denote the overlapping partitioning of  $\Omega$  such that  $\Omega_j \subset \Omega'_j$ . In practice, each  $\Omega'_j$  is constructed by propagating  $\Omega_j$  by a few layers of triangles. With this, let  $R_j$  denote the boolean restriction matrices which restrict from the degrees of freedom in the discretization of  $\Omega$  to the degrees of freedom in the overlapping subdomain  $\Omega'_j$ , and let  $D_j$  denote partition of unity matrices corresponding to the discretization of  $\Omega'_j$  such that  $\sum_{j=1}^N R_j^T D_j R_j = I$ .

With this, the iterative RAS method computes the approximation to the solution  $\mathbf{u}^{k+1}$  from  $\mathbf{u}^k$  by

$$\mathbf{u}^{k+1} = \mathbf{u}^k + M_{RAS,1}^{-1}(\mathbf{f} - A\mathbf{u}^k), \quad (10)$$

where

$$M_{RAS,1}^{-1} = \sum_{j=1}^N R_j^T D_j [R_j A R_j^T]^{-1} R_j.$$

Additionally, we can accelerate this fixed-point method (10) by solving the preconditioned system

$$M_{RAS,1}^{-1} A \mathbf{u} = M_{RAS,1}^{-1} \mathbf{f}, \quad (11)$$

with a Krylov type method such as GMRES.

Generally, the number of iterations in (10) and (11) grows with the number of subdomains in one direction. For example, this increase is linear for the stationary iteration (10). To combat this, a coarse level is needed to aid in global communication between all subdomains. Consider the coarse matrix  $R_H$  defined in Section 3; with this, the two-level preconditioned Krlov method method is given by

$$M_{RAS,2}^{-1} A \mathbf{u} = M_{RAS,2}^{-1} \mathbf{f}, \quad (12)$$

where

$$M_{RAS,2}^{-1} = R_H^T (R_H A R_H^T)^{-1} R_H + \sum_{j=1}^N R_j^T D_j [R_j A R_j^T]^{-1} R_j. \quad (13)$$

## 5. Nonlinear Multi-domain Solution Methods

We present results for various methods to solve the nonlinear system  $F(\mathbf{u}) = 0$ , where  $F(\mathbf{u})$  arises from some discretization of a nonlinear PDE. For the Diffusive Wave model, the residual function  $F(\mathbf{u}) = 0$  is given in (5).

*Preconditioning the linearized Newton system.* To solve nonlinear equations, Newton's method is commonly employed. For exact Newton's method, one needs the the residual  $F(\mathbf{u})$  as well as the Jacobian  $\nabla F(\mathbf{u})$ . The exact Newton's method is described in Algorithm 1.

---

**Algorithm 1** Newton's method to solve  $F(\mathbf{u}) = 0$

---

**Require:**  $\mathbf{u}^0$ , residual function  $F$ , Jacobian  $\nabla F$   
**for**  $k = 0, \dots$ , to convergence **do**  
    Compute Newton update  $\boldsymbol{\delta} = [\nabla F(\mathbf{u})]^{-1} F(\mathbf{u})$   
    Compute  $\mathbf{u}^{k+1} = \mathbf{u}^k - \boldsymbol{\delta}$ ;  
**end for**

---

Often when implementing Newton's method, a backtracking line search is implemented to control the step size of Newton's method. This often aids in convergence for certain problems as the line search prevents "overshooting" in the Newton step direction. Newton's method with backtracking line search is given in Procedure 1.

---

**Procedure 1** Newton's Method with backtracking line search to solve  $F(\mathbf{u}) = 0$

---

**for**  $k = 0, \dots$ , to convergence **do**  
     $d = 1$   
    Compute Newton update  $\boldsymbol{\delta} = [\nabla F(\mathbf{u})]^{-1} F(\mathbf{u})$   
    **while**  $\|F(\mathbf{u} - d\boldsymbol{\delta})\| > (1 - \frac{d}{4})\|F(\mathbf{u})\|$  **do**  
         $d = \frac{d}{2}$   
    **end while**  
    Compute  $\mathbf{u}^{k+1} = \mathbf{u}^n - d\boldsymbol{\delta}$ ;  
**end for**

---

When a linear system is very large, a direct solve is often too expensive and not recommended. Therefore, it is common to solve the linear system in Algorithm 1 via a preconditioned Krylov solver. We proposed in [4] and recalled in Section 3 a coarse space for the two-level RAS preconditioner applied to the Poisson equation on perforated domains. It turns out that the same coarse space can be successfully employed within the two-level RAS

preconditioner (13) for the linear system in Algorithm 1. The numerical evidences regarding the efficiency of such a two-level solver are presented in Section 6.

Let  $J_k = \nabla F(\mathbf{u}^k)$  denote the Jacobian matrix and  $\mathbf{F}_k = F(\mathbf{u}^k)$  the residual at a given iterate. The Newton's method update denoted by  $\boldsymbol{\delta}_k$  satisfies the system

$$J_k \boldsymbol{\delta}_k = \mathbf{F}_k.$$

The preconditioned system to solve for  $\boldsymbol{\delta}_k$  is as follows:

$$M_{RAS,2}^{-1} J_k \boldsymbol{\delta}_k = M_{RAS,2}^{-1} \mathbf{F}_k,$$

where  $M_{RAS,2}$  is defined as in (13) with system matrix  $A$  replaced by  $J_k$ ,

$$M_{RAS,2}^{-1} = \sum_{j=1}^N R_j^T D_j (R_j J_k R_j^T)^{-1} R_j + R_H^T (R_H J_k R_H^T)^{-1} R_H. \quad (14)$$

*Nonlinear Restrictive Additive Schwarz Iteration.* Recall for linear systems  $A\mathbf{u} = \mathbf{f}$ , the Restricted Additive Schwarz (RAS) method can be used as an iterative method or as a preconditioner for Krylov methods. Likewise, for the nonlinear problem, we introduce a nonlinear RAS (NRAS) fixed point iteration. Multiple methods which are to be introduced will require this nonlinear RAS iteration.

An NRAS iteration is computed by first solving a nonlinear subsystem corresponding to  $\Omega'_j$  then gluing these local subdomain updates together. Let  $R_j$  be the boolean restriction matrices corresponding to the degrees of freedom of  $\Omega'_j$ ; we introduce the “subdomain update” function  $G_j$ , such that, for all  $\mathbf{u}$ ,  $G_j(\mathbf{u})$  is the solution of

$$R_j F(R_j^T G_j(\mathbf{u}) + (I - R_j^T R_j)\mathbf{u}) = 0. \quad (15)$$

The subdomain updates  $G_j(\mathbf{u})$  correspond to solving the problem on  $\Omega'_j$  with Dirichlet boundary conditions. The local problems (15) are solved via Newton's method; as the subproblems are small, each Newton linear system is solved using a direct solver. Then, the local solutions  $G_j(\mathbf{u})$  are glued together, giving the global update function

$$\text{NRAS}(\mathbf{u}) = \sum_j R_j^T D_j G_j(\mathbf{u}). \quad (16)$$

We remark that, in principle, as in the linear case, we can use this nonlinear RAS method as a fixed point iteration, giving

$$\mathbf{u}^{k+1} = \text{NRAS}(\mathbf{u}^k). \quad (17)$$

As a quick remark, we comment on the connection between the nonlinear RAS fixed point iteration (17) and the linear RAS fixed point iteration (10). Consider the local solutions computed from (15). For linear problems such that  $F(\mathbf{u}) = A\mathbf{u} - \mathbf{f}$ , we have

$$\begin{aligned} R_j F(R_j^T G_j(\mathbf{u}) + (I - R_j^T R_j)\mathbf{u}) &= 0 \\ R_j (A(R_j^T G_j(\mathbf{u}) + (I - R_j^T R_j)\mathbf{u}) - \mathbf{f}) &= 0 \\ R_j A R_j^T G_j(\mathbf{u}) &= R_j A R_j^T R_j \mathbf{u} + R_j (\mathbf{f} - A\mathbf{u}) \\ G_j(\mathbf{u}) &= R_j \mathbf{u} + (R_j A R_j^T)^{-1} R_j (\mathbf{f} - A\mathbf{u}) \end{aligned} \quad (18)$$

such that the fixed point iteration (17) would be equivalent to

$$\begin{aligned}
\mathbf{u}^{k+1} &= \sum_{j=1}^N R_j^T D_j (R_j \mathbf{u}^k + (R_j A R_j^T)^{-1} R_j (\mathbf{f} - A \mathbf{u}^k)) \\
&= \mathbf{u}^k + \sum_{j=1}^N R_j^T D_j (R_j A R_j^T)^{-1} R_j (\mathbf{f} - A \mathbf{u}^k) \\
&= \mathbf{u}^k + M_{RAS,1}^{-1} (\mathbf{f} - A \mathbf{u}^k),
\end{aligned} \tag{19}$$

where we have used the partition of unity property  $I = \sum_{j=1}^N R_j^T D_j R_j$ . Therefore, the NRAS fixed point iteration (17) reduces to the linear RAS fixed point iteration (10).

*One-level RASPEN.* Recall that in the linear case, we can accelerate the fixed point RAS iteration by Krylov methods. Analogously, in the nonlinear case, we can accelerate the NRAS fixed point iteration (17) by applying Newton's method to the fixed point equation

$$\mathcal{F}(\mathbf{u}) := \mathbf{u} - \text{NRAS}(\mathbf{u}) = 0$$

resulting in one-level RASPEN method [13] detailed in Algorithm 2. It was shown in [13] that the Jacobian of  $\mathcal{F}(\mathbf{u})$  can be computed directly.

---

**Algorithm 2** One-level RASPEN to solve  $F(\mathbf{u}) = 0$

---

**Require:**  $\mathbf{u}^0$ , residual function  $F$ , Jacobian  $\nabla F$

**for**  $k = 0, \dots$ , to convergence **do**

    Compute NRAS update  $\hat{\mathbf{u}}^k = \text{NRAS}(\mathbf{u}^k)$ ;

    Set  $\mathcal{F}(\mathbf{u}^k) = \mathbf{u}^k - \hat{\mathbf{u}}^k$

    Solve  $\mathbf{u}^{k+1} = \mathbf{u}^k - [\nabla \mathcal{F}(\mathbf{u}^k)]^{-1} \mathcal{F}(\mathbf{u}^k)$ .

**end for**

In other words, solve  $\mathcal{F}(\mathbf{u}) = 0$  via Newton's method.

---

We now describe the computation of the Jacobian  $\nabla \mathcal{F}(\mathbf{u}^k)$  for Algorithm 2. In view of (16), we have

$$\mathcal{F}(\mathbf{u}^k) = \mathbf{u}^k - \text{NRAS}(\mathbf{u}^k) = \mathbf{u}^k - \sum_j R_j^T D_j G_j(\mathbf{u}^k).$$

Then the Jacobian is given by

$$\begin{aligned}
\nabla \mathcal{F}(\mathbf{u}^k) &= \nabla \left( \mathbf{u}^k - \sum_j R_j^T D_j G_j(\mathbf{u}^k) \right) \\
&= I - \sum_j R_j^T D_j \nabla G_j(\mathbf{u}^k)
\end{aligned} \tag{20}$$

Therefore, to compute the Jacobian  $\nabla[\mathcal{F}(\mathbf{u}^k)]$ , we must compute  $\nabla G_j(\mathbf{u}^k)$ . To compute  $\nabla G_j(\mathbf{u}^k)$ , recall (15). Taking the derivative of this equation and solving for  $\nabla G_j(\mathbf{u}^k)$  gives

$$\nabla G_j(\mathbf{u}^k) = R_j - [R_j \nabla F(\mathbf{v}_j^k) R_j^T]^{-1} R_j \nabla F(\mathbf{v}_j^k) \quad (21)$$

where we have set  $\mathbf{v}_j^k = R_j^T G_j(\mathbf{u}^k) + (I - R_j^T R_j) \mathbf{u}^k$  for convenience. Thus, we have

$$\begin{aligned} \nabla \mathcal{F}(\mathbf{u}^k) &= I - \sum_j R_j^T D_j \nabla G_j(\mathbf{u}^k), \\ &= I - \sum_j R_j^T D_j (R_j - [R_j \nabla F(\mathbf{v}_j^k) R_j^T]^{-1} R_j \nabla F(\mathbf{v}_j^k)), \\ &= \sum_j R_j^T D_j [R_j \nabla F(\mathbf{v}_j^k) R_j^T]^{-1} R_j \nabla F(\mathbf{v}_j^k), \end{aligned} \quad (22)$$

where we have used the partition of unity property  $I = \sum_j R_j^T D_j R_j$ . We note that the inverse  $[R_j \nabla F(\mathbf{v}_j^k) R_j^T]^{-1}$  can be dense matrix. Therefore, we set up  $\nabla \mathcal{F}(\mathbf{u}^k)$  as a linear operator, allowing us to compute the matrix-vector product  $\nabla \mathcal{F}(\mathbf{u}^k) x^k$  for any vector  $x^k$  without explicitly computing the matrix  $\nabla \mathcal{F}(\mathbf{u}^k)$ .

*Two-level RASPEN.* It is well-known that one-level domain decomposition methods are not scalable with respect to the number of subdomains. Specifically, the GMRES method used at each outer iteration of Algorithm 2 is not scalable without a coarse level. Therefore, we implement a two-level RASPEN variant.

We choose a multiplicative two-level RASPEN correction provided in [19], which allows the coarse correction to be done algebraically. The authors of [15] provide numerical experiments on multiple different choices of two-level methods, including adding the coarse correction before, after, and before and after the nonlinear RAS iteration. The multiplicative two-level RASPEN method we have chosen is given by Algorithm 3. This method solves the nonlinearly preconditioned system

$$\mathcal{F}(\mathbf{u}) = \mathbf{u} - \text{NRAS}(\mathbf{u}) + R_H^T c_H(\text{NRAS}(\mathbf{u})), \quad (23)$$

where the function  $c_H(\mathbf{v})$  for a given  $\mathbf{v}$  is defined as the solution to the “coarse” nonlinear equation

$$R_H F(\mathbf{v} - R_H^T c_H(\mathbf{v})) = 0. \quad (24)$$

*Two-step method.* Next, we consider a Two-step method proposed in [9] under the name NKS-RAS; see also [5]. This method alternates between an NRAS iteration and a global Newton step at each outer iteration. This method leads to fast convergence (typically quadratic convergence is expected), but unlike Algorithms 2 and 3, can not be framed as a nonlinear preconditioning method. The Two-step method is given in Algorithm 4. The main feature of the Two-step method is the ease of its implementation. Compared to the standard Newton’s method, it simply requires an additional NRAS step; moreover, compared to one and two-level RASPEN, the two-step method does not involve any dense linear systems, and therefore, in principle, may be implemented based on a direct linear solver. Here, the linearized system of Algorithm 4 is solved using the same preconditioned GMRES method as in Algorithm 1.

---

**Algorithm 3** Two-level RASPEN to solve  $F(\mathbf{u}) = 0$ 

---

**Require:**  $\mathbf{u}^0$ , residual function  $F$ , Jacobian  $\nabla F$

**for**  $k = 0, \dots$ , to convergence **do**

    Compute NRAS update  $\hat{\mathbf{u}}^k = \text{NRAS}(\mathbf{u}^k)$ ;

    Solve coarse problem  $R_H F(\hat{\mathbf{u}}^k - R_H^T c_H(\hat{\mathbf{u}}^k)) = 0$  for  $c_H(\hat{\mathbf{u}}^k)$  via Newton's method;

    Set  $\mathcal{F}(\mathbf{u}^k) = \mathbf{u}^k - \hat{\mathbf{u}}^k + R_H^T c_H(\hat{\mathbf{u}}^k)$ ;

    Solve  $\mathbf{u}^{k+1} = \mathbf{u}^k - [\nabla \mathcal{F}(\mathbf{u}^k)]^{-1} \mathcal{F}(\mathbf{u}^k)$ .

**end for**

In other words, solve  $\mathcal{F}(\mathbf{u}) = 0$  via Newton's method.

---

---

**Algorithm 4** Two-step method to solve  $F(\mathbf{u}) = 0$ 

---

**Require:**  $\mathbf{u}^0$ , residual function  $F$ , Jacobian  $\nabla F$

**for**  $k = 0, \dots$ , to convergence **do**

    Compute NRAS update  $\hat{\mathbf{u}}^k = \text{NRAS}(\mathbf{u}^k)$ ;

    Compute Newton update  $\mathbf{u}^{k+1} = \hat{\mathbf{u}}^k - [\nabla F(\hat{\mathbf{u}}^k)]^{-1} F(\hat{\mathbf{u}}^k)$ ;

**end for**

---

*Anderson Acceleration of Coarse Two-step Method.* The two-step method given in Algorithm 4 involved a global fine-scale linear solve at each outer iteration. We now propose to replace this step with a “coarse” linear solve, using the Trefftz coarse space described in Section 3. For this, we can employ a method similar to the two-step method (4) but with a “coarse” Newton step at each iteration, in a method similar to our previous works on linear models. We refer to this as the Coarse Two-Step method, which allows us to use the coarse Trefftz space in the iteration and cheapen the cost of the global Newton update. This Coarse Two-step method is a fixed point iteration which involves a coarse Newton update, which we denote by

$$F_c(\mathbf{u}) = \mathbf{u} - R_H^T \delta_H, \quad \text{where} \quad \delta_H = [R_H \nabla F(\mathbf{u}) R_H^T]^{-1} R_H F(\mathbf{u}). \quad (25)$$

With this, the fixed point coarse two-step method is given as follows: for iteration  $k = 0, 1, \dots$ , to convergence, compute

$$\begin{aligned} \hat{\mathbf{u}}^k &= \text{NRAS}(\mathbf{u}^k), \\ \mathbf{u}^{k+1} &= F_c(\hat{\mathbf{u}}^k). \end{aligned} \quad (26)$$

The convergence of the fixed point method (26) to the numerical solution is generally quite slow when compared to the original Two-step method given by Algorithm 4, as a full update is not done at each iteration. To combat this, we introduce Anderson Acceleration [28] as a way to accelerate the fixed point method (26), resulting in Algorithm 5. The general Anderson acceleration method is given in Procedure 2. Given some  $\mathbf{u}^{k+1} = P(\mathbf{u}^k)$ , we solve  $\mathcal{F}(\mathbf{u}) = P(\mathbf{u}) - \mathbf{u} = 0$  via Anderson acceleration. While the parameter  $m_k$  in Algorithm 2 can vary, we generally choose  $m_k = 10$  in our numerical experiments and do not explore this parameter further. For convenience, we will refer to the Anderson Acceleration of the Coarse Two-step method (Algorithm 5) as the “Anderson method” for the duration of the article.

We note that Anderson's method generally fails to accelerate quadratically convergent fixed point iterations; this is proven with an error estimate in [14].

---

**Algorithm 5** Anderson Acceleration Applied to Coarse two-step method to solve  $F(\mathbf{u}) = 0$

---

**Require:**  $\mathbf{u}^0$ , residual function  $F$ , Jacobian  $\nabla F$

Denote  $F_c(\mathbf{u}) := \mathbf{u} - R_H^T[R_H \nabla F(\mathbf{u}) R_H^T]^{-1} R_H F(\mathbf{u})$ ;

Solve  $V(\mathbf{u}) := F_c(\text{NRAS}(\mathbf{u})) = 0$  by Anderson acceleration, (Procedure 2).

The solution to  $V(\mathbf{u}) = 0$  is the solution to  $F(\mathbf{u}) = 0$ .

---



---

**Procedure 2** Anderson Acceleration to solve some general function of the form  $V(\mathbf{u}) = P(\mathbf{u}) - \mathbf{u} = 0$

---

**Require:**  $\mathbf{u}^0$  and  $m \geq 1$

Set  $\mathbf{u}^1 = P(\mathbf{u}^0)$ ;

**for**  $k = 1, 2, \dots$ , to convergence **do**

Set  $m_k = \min\{m, k\}$ ;

Set  $f_k = (\mathbf{V}_{k-m_k}, \dots, \mathbf{V}_k)$ , where  $\mathbf{V}_i = P(\mathbf{u}^i) - \mathbf{u}^i$ ;

Determine  $\alpha^k = (\alpha_0^k, \dots, \alpha_{m_k}^k)^T$  that solves

$$\min_{\alpha^k = (\alpha_0^k, \dots, \alpha_{m_k}^k)^T} \|f_k \alpha^k\|_2 \quad \text{such that} \quad \sum_{i=0}^{m_k} \alpha_i^k = 1;$$

Update  $\mathbf{u}^{k+1}$  using Anderson mixing:  $\mathbf{u}^{k+1} = \sum_{i=0}^{m_k} \alpha_i^k P(\mathbf{u}^{k-m_k+i})$ ;

**end for**

---

### 5.1. Complexities/Costs of Fine-scale Methods

We now provide an overview of the complexity of each method. To quantify the cost of each algorithm, we recall that at each time step, each outer iteration consists of the following for each method:

- Newton: 1 global Newton update (1 global two-level linearly preconditioned Krylov solve);
- Two-Step: 1 NRAS Update + 1 global Newton update (1 global two-level linearly preconditioned Krylov solve);
- One-level RASPEN: 1 NRAS update + 1 global Newton update (1 one-level nonlinearly preconditioned Krylov solve);
- Two-level RASPEN: 1 NRAS update + 1 coarse nonlinear solve + 1 global Newton update (1 two-level nonlinearly preconditioned Krylov solve);
- Anderson: 1 NRAS update + 1 coarse linear solve + 1 small least-squares problem.

Computing the NRAS update (16) requires solving a family of local nonlinear systems associated to the subdomains. The local nonlinear systems are computed by Newton's method, with a linear system solved at each iteration. We denote by  $N_{it,loc}$  the required number of local Newton iterations averaged over all subdomains. Due to the small size of the subdomains, the linearized system at each Newton iteration is computed via a direct sparse linear solve. We denote by  $C(LU_{loc})$  a typical cost of the local LU decompositions on each subdomain, assumed to be approximately the same for every subdomain. The complexity of the NRAS iteration can be expressed by

$$C(\text{NRAS}) \approx N \cdot C(LU_{loc})N_{it,loc}, \quad (27)$$

Here, (27) assumes that the local computations are not done in parallel.

With the exception of Anderson's method, all methods involve a global linear system which is solved via GMRES. The complexity of the GMRES method is given by

$$N \cdot C(LU_{loc}) + N_{\text{GM}}C(\text{GMRES}),$$

where  $N \cdot C(LU_{loc})$  denotes the one-time cost of assembling the preconditioner and  $C(\text{GMRES})$  denotes the cost of each GMRES iteration, which is generally involves a sparse matrix-vector multiplication. We note that in the RASPEN variants, the LU decompositions can be reused from the earlier NRAS iteration; this would slightly reduce the cost further. We denote by  $C(\text{coarse})$  the cost of the sparse linear solve (25). Therefore,  $N_c C(\text{coarse})$  denotes the total cost of the coarse nonlinear problems in the two-level RASPEN algorithm (Algorithm 3), where  $N_c$  denotes the number of coarse linear solves.

Furthermore, we quantify the following costs:

- $C(LU_{loc}) = O(N_{loc}^{3/2})$ , where  $N_{loc} \approx \frac{N_\Omega}{N}$  denotes the number of degrees of freedom in a subdomain and is assumed to be roughly consistent over all subdomains;
- $C(\text{GMRES}) = O(N_\Omega)$  for each sparse matrix-vector product;
- $C(\text{coarse}) = O(N_V^{3/2})$ ;

where the LU decomposition of some sparse  $m \times m$  matrix is supposed to be  $O(m^{3/2})$  [16]. Finally, *for each outer iteration*, each method has the following cost:

$$\begin{aligned} C(\text{Newton}) &\approx N \cdot O(N_{loc}^{3/2}) + N_{\text{GM}}O(N_\Omega); \\ C(\text{Two-Step}) &\approx N \cdot O(N_{loc}^{3/2})N_{it,loc} + N \cdot O(N_{loc}^{3/2}) + N_{\text{GM}}O(N_\Omega); \\ C(\text{One-RASPEN}) &\approx N \cdot O(N_{loc}^{3/2})N_{it,loc} + N \cdot O(N_{loc}^{3/2}) + N_{\text{GM}}O(N_\Omega); \\ C(\text{Two-RASPEN}) &\approx N \cdot O(N_{loc}^{3/2})N_{it,loc} + N \cdot O(N_{loc}^{3/2}) + N_{\text{GM}}O(N_\Omega) + N_c O(N_V^{3/2}); \\ C(\text{Anderson}) &\approx N \cdot O(N_{loc}^{3/2})N_{it,loc} + O(N_\Omega) + O(N_V^{3/2}); \end{aligned}$$

where the  $O(N_\Omega)$  term arises as the dominant term in the least-squares problem of Anderson's method. Clearly, the values  $N_{it,loc}$ ,  $N_{\text{GM}}$ ,  $N_c$  and the total number of outer iterations can not be known a priori. In Section 6, we record the number of GMRES iterations  $N_{\text{GM}}$ , the number of local linear NRAS iterations averaged over all subdomains  $N_{it,loc}$ , and the total number of coarse linear iterations  $N_c$ , as well as the total number of outer iterations.



## 6. Numerical Results

We now proceed with numerical experiments for the proposed algorithms for multiple test cases. These numerical tests will proceed in order of increasing difficulty; they include a porous media equation on an L-shaped domain, a porous media equation on a smaller realistic urban domain, and the Diffusive Wave model on a large realistic urban domain. As mentioned, the fine-scale triangulation is conforming to the coarse polygonal partitioning. For the numerical tests on urban areas (Examples 2 and 3), we ensure that the fine-scale triangulation is identical as the number of subdomains  $N$  changes by generating a finer background mesh to be used for various  $N$ ; for example, we can generate a fine-scale triangulation for  $N = 16 \times 16$  subdomains, then use this background triangulation for  $N = 2 \times 2, 4 \times 4$ , or  $8 \times 8$  subdomains. Figure 6 shows a matching background triangulation for  $N = 2 \times 4$  and  $8 \times 16$  subdomains, respectively.

For all numerical experiments, the overlap is set to  $\frac{1}{20}\mathcal{H}_j$ , where  $\mathcal{H}_j = \max(x_{\max,j} - x_{\min,j}, y_{\max,j} - y_{\min,j})$  and  $x_{\min,j}, y_{\min,j}, x_{\max,j}, y_{\max,j}$  denote the minimal and maximal  $x$  and  $y$  coordinates that are contained in  $\Omega_j$ . We do not explore the effect of overlap further.

### 6.1. Porous Media Equation on L-shaped Domain

As a first numerical example, referred to as Example 1, we use an L-shaped domain with a reentering corner. The domain is defined by  $D = (-1, 1)^2$ ,  $\Omega_S = (0, 1)^2$  and  $\Omega = D \setminus \overline{\Omega_S}$  such that the model domain has singularity/corner in the upper right quadrant of the domain. With this model domain, we consider a porous media equation given by

$$\left\{ \begin{array}{lll} u(x, y) + \operatorname{div}(\nabla(u(x, y)^4)) & = & 0 \quad \text{in } \Omega, \\ u(x, y) & = & 1 \quad \text{on } y = 1, \\ u(x, y) & = & 0 \quad \text{on } x = 1, \\ \frac{\partial u(x, y)}{\partial \mathbf{n}} & = & 0 \quad \text{on } \Gamma_N, \end{array} \right. \quad (28)$$

where  $\Gamma_N = \{(x, y) \in \partial\Omega \mid x \neq 1 \text{ and } y \neq 1\}$  denotes the Neumann boundary. Consider a piecewise affine finite element discretization and let  $\mathbf{u}$  denote a vector of interior node values of size  $N_\Omega$ . We denote the nodal ‘‘hat’’ basis functions  $(\eta^\ell)_{\ell=1}^{N_\Omega}$ . We define the lumped finite-element mass matrix  $M$  and finite element stiffness matrix  $A$  such that

$$M_{ii} = \sum_{\ell=1}^{N_\Omega} \int_{\Omega} \eta_i \eta_\ell \, d\mathbf{x}, \quad \text{and} \quad A_{i\ell} = \int_{\Omega} \nabla \eta_i \cdot \nabla \eta_\ell \, d\mathbf{x}.$$

With this, the matrix-vector notation of (28) becomes

$$F(\mathbf{u}) = M\mathbf{u} + A\phi, \quad (29)$$

where

$$\phi = \max(\mathbf{u}, 0)^4.$$

The finite element solution of this equation is shown in Figure 2.

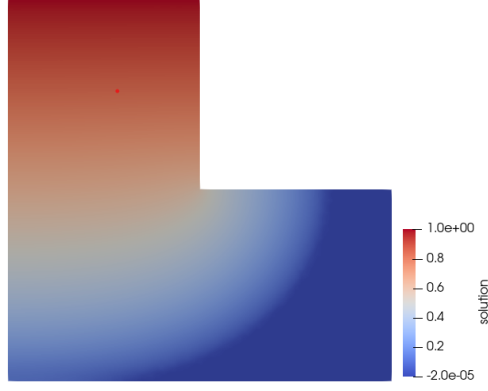


Figure 2: Finite element solution of (28) for Example 1 on the chosen L-shaped domain.

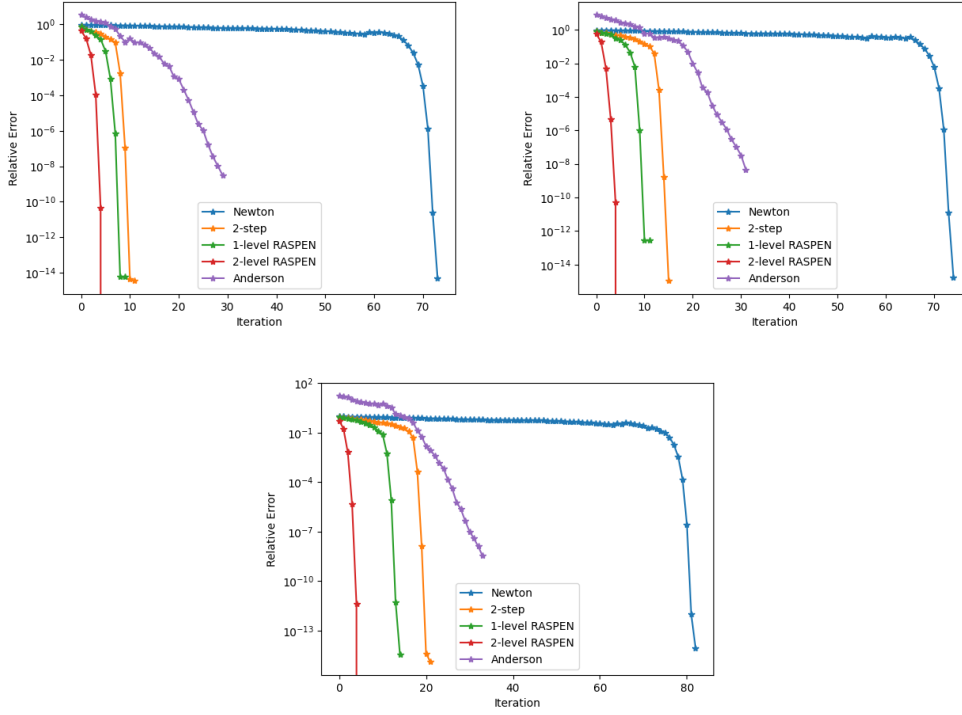


Figure 3: Example 1, convergence curves. Top:  $N = 3$  (left),  $N = 5$  (right). Bottom:  $N = 9$ .

Method	Outer Its	GMRES Its (per outer it)	$N_{it,loc}$
Newton	88	38.1	N/A
Anderson	31	N/A	4.35
2-step	22	35.0	3.96
1-level RASPEN	15	85.3	3.7
2-level RASPEN	6	19.2(+5.3 coarse)	3.94

Table 1: Example 1,  $N = 9$ , initial guess  $\mathbf{u}^0 = 0.05$ .

Method	Outer Its	GMRES Its (per outer it)	$N_{it,loc}$
Newton	81	33.4	N/A
Anderson	32	N/A	4.64
2-step	16	34.0	4.86
1-level RASPEN	11	53.9	5.08
2-level RASPEN	6	19.2(+4.5 coarse)	4.48

Table 2: Example 1,  $N=5$ , initial guess  $\mathbf{u}^0 = 0.05$ .

Method	Outer Its	GMRES Its (per outer it)	$N_{it,loc}$
Newton	79	33.7	N/A
Anderson	25	N/A	4.36
2-step	13	38.9	6.06
1-level RASPEN	9	35.4	6.96
2-level RASPEN	6	20.5(+3.8 coarse)	5.5

Table 3: Example 1,  $N=3$ , initial guess  $\mathbf{u}^0 = 0.05$ .

We provide numerical results for this example for Newton's method given by Algorithm 1, the two-step method from Algorithm 4, the one-level RASPEN method from Algorithm 2, the two-level RASPEN method from Algorithm 3, and the Anderson acceleration method from Algorithm 5. For the two-step and Newton methods, at each outer iteration, the linear system is solved using GMRES method combined with the linear two-level RAS preconditioner (14). We show results for coarse partitionings  $N = 9 \times 9$ ,  $5 \times 5$ , and  $3 \times 3$ ; The choice of  $N$  being a

square of an odd number ensures the consistency of the mesh sequence in terms of the shape of the elements.

Convergence curves for this example are shown in Figure 3. Additionally results for this example are summarized in Tables 1, 2, and 3. These tables report the total number of outer iterations and, whenever appropriate, also report the number of GMRES and NRAS iterations. From Figure 3, we see that Newton's method results in a very large plateau before the region of quadratic convergence is reached. This difference is stark when compared to the other methods. Additionally, for all number of subdomains  $N$ , two-level RASPEN outperforms the other methods in terms of iteration count, with one-level RASPEN, two-step, and Anderson acceleration following in order. Additionally, we notice that while Anderson does not plateau like Newton's method, we do not obtain the eventual steep slope of convergence which the other methods achieve.

We see from Tables 1, 2, and 3 that the two-level RASPEN method is consistently resulting in fewer iterations than the other methods regardless of the number of subdomains  $N$ . The two-level RASPEN method is almost perfectly scalable based on the number of outer and GMRES iterations. We observe that the one-level RASPEN method loses scalability in terms of GMRES iterations as the number of subdomains increases, more so than the other methods which all involve a coarse component of some type. We also observe that Newton's method and the Two-step method, which both solve a linearized system with the linear two-level RAS preconditioner (with the Trefftz space as the coarse space), result in fair scalability in terms of GMRES iterations. However, both methods still result overall in more GMRES iterations per outer iteration. We additionally remark that the two-step method and Newton's method result in around the same number of GMRES iterations per outer iteration, with the two-step method resulting in fewer outer iterations than Newton's method.

## 6.2. Porous Media Equation on Large Urban Domain

As a second example, referred to as Example 2, we provide numerical results for a Porous Media equation on a large urban domain of size  $160 \times 160$  metres such that  $D = (-80, 80)^2$  and  $\Omega_S$  is given by the union of realistic perforations. The buildings are removed from the computational domain, leading to 72 total perforations. The geometry of the buildings have been provided by M  tropole Nice C  te d'Azur. After discretization, this model domain contains 35220 triangles and 21317 mesh points. As mentioned, the overlap is set to  $\frac{1}{20}\mathcal{H}_j$ .

With this, we consider a porous media equation given by

$$\left\{ \begin{array}{llll} u(x, y) + c \operatorname{div}(\nabla(u(x, y)^m)) & = & 0 & \text{in } \Omega, \\ u(x, y) & = & c & \text{on } x = -80, \\ u(x, y) & = & 0 & \text{on } x = 80, \\ \frac{\partial u(x, y)}{\partial \mathbf{n}} & = & 0 & \text{on } \Gamma_N, \end{array} \right. \quad (30)$$

where  $\Gamma_N = \{(x, y) \in \partial\Omega \mid x \neq -80 \text{ and } y \neq 80\}$  denotes the Neumann boundary; with this, the boundary of each perforation ( $\partial\Omega \cap \Omega_S$ ) is included in  $\Gamma_N$ . Here, we take  $m = 3$  and  $c = 15$  in (30). The finite element solution for this example is shown in Figure 4.

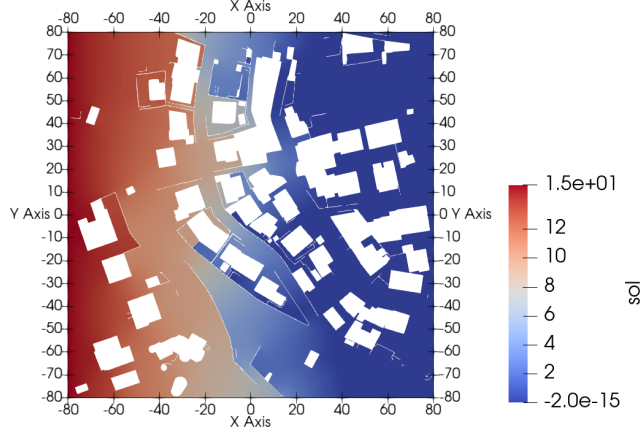


Figure 4: Finite element solution of (28) for Example 2 on the chosen urban model domain.

For this example, we provide numerical results for Newton’s method from Algorithm 1, the two-step method from Algorithm 4, the two-level RASPEN method from Algorithm 3, and the Anderson acceleration method from Algorithm 5. As we have established that one-level RASPEN is not a scalable method for large  $N$ , we do not provide results for one-level RASPEN in this example. As in the previous example, for the two-step and Newton methods, at each outer iteration, the linear system is solved using GMRES method combined with the linear two-level RAS preconditioner (14).

The results for this example are summarized in Tables 4, 5, 6, and 7 for initial guesses of  $\mathbf{u}^0 = 1$  and  $\mathbf{u}^0 = 0$  and for subdomain partitioning of  $N = 16 \times 16, 8 \times 8, 4 \times 4$ , and  $2 \times 2$ , respectively. As mentioned, while the coarse partitionings vary, the background fine-scale triangulation is consistent throughout the numerical experiment. The total number of coarse nodes are given by  $N_V = 784, 332, 149$ , and  $56$  for  $N = 16 \times 16, 8 \times 8, 4 \times 4$ , and  $2 \times 2$ , respectively.

Corresponding convergence curves for both initial guesses are provided in Figure 5. Even more than the previous example, Newton’s method has a large plateau in convergence before reaching the region of quadratic convergence. In terms of initial guess, we observe that Newton’s method is much more sensitive to the initial guess than the other methods in terms of outer iteration count. In fact, we see that this change in initial guess can result in a 50% increase in iteration count for Newton’s method. Other than the outer iterations for Newton’s method, there is not much dependence on the initial guess. For all number of subdomains  $N$ , two-level RASPEN outperforms the other methods in terms of iteration count, with the Two-step, Anderson, and Newton’s methods following in increasing order. We particularly see that the outer iterations of the two-level RASPEN method are extremely robust with respect to  $N$ , more so than the other accelerated methods.

From Tables 4, 5, 6, and 3, we see again that all two-level algorithms are fairly scalable in terms of GMRES iterations, with the two-level RASPEN method having the fewest GMRES iterations per iteration and the fewest outer iterations. The two-level RASPEN method is almost perfectly scalable in terms of GMRES and outer iterations. Again, the Two-step method and Newton’s method result in around the same number of GMRES iterations per

outer iteration, with the two-step method resulting in fewer outer iterations than Newton's method. Overall, our conclusions from Example 2 are similar to that of Example 1, with Newton's method particularly struggling in terms of outer iterations and having the most dependency on the initial guess. However, in terms of solving the linearized system, it appears that the Trefftz coarse space is successful as a component of the linear two-level RAS preconditioner for this nonlinear problem.

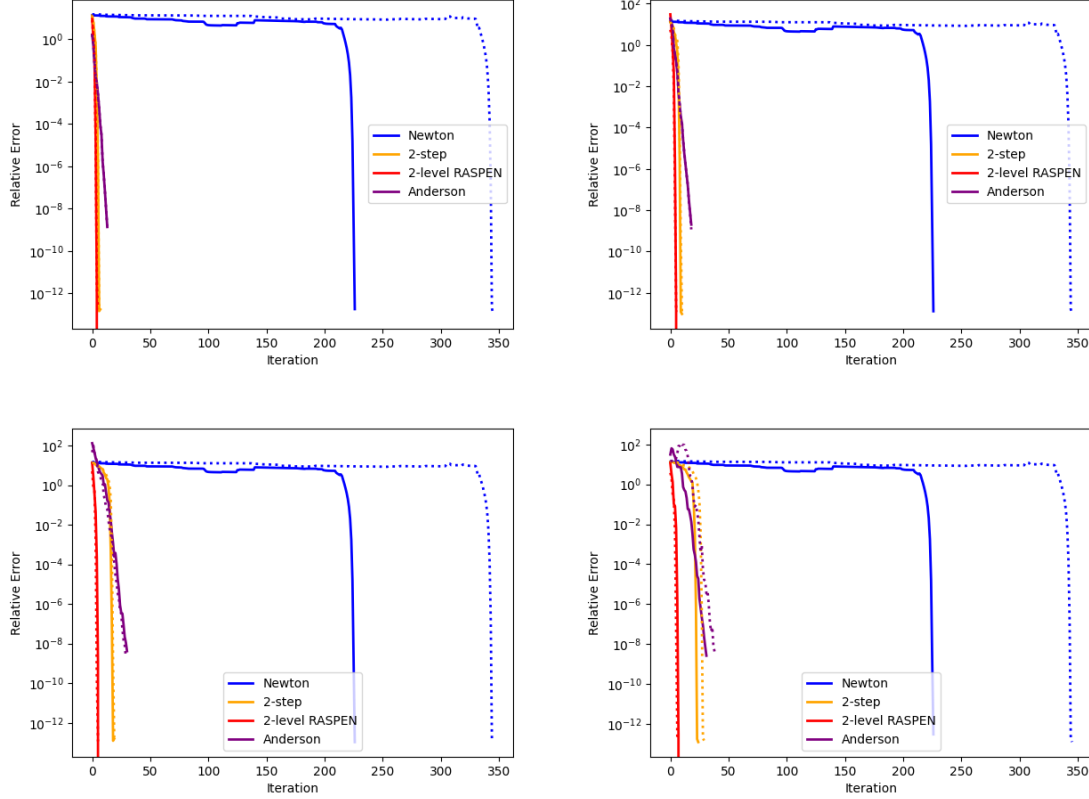


Figure 5: Example 2, convergence curves. Solid lines correspond to an initial guess of  $\mathbf{u}^0 = 1$ , dotted lines correspond to an initial guess of  $\mathbf{u}^0 = 0$ . Top:  $N = 2 \times 2$  (left),  $N = 4 \times 4$  (right). Bottom:  $N = 8 \times 8$  (left),  $N = 16 \times 16$  (right).

Method	Its		GMRES Its (per it)		$N_{it,loc}$	
	$\mathbf{u}^0 = 1$	$\mathbf{u}^0 = 0$	$\mathbf{u}^0 = 1$	$\mathbf{u}^0 = 0$	$\mathbf{u}^0 = 1$	$\mathbf{u}^0 = 0$
Newton	227	346	45.0	46.0	N/A	N/A
Anderson	37	52	N/A	N/A	4.1	5.07
2-step	25	30	41.1	41.6	4.14	2.83
2-RASPEN	9	8	22.3(+7.4)	19.2 (+9.6)	3.13	2.11

Table 4: Example 2,  $N = 16 \times 16$  subdomains, results for two different initial guesses  $\mathbf{u}^0 = 0$  and  $\mathbf{u}^0 = 1$ .

Method	Its		GMRES Its (per it)		$N_{it,loc}$	
	$\mathbf{u}^0 = 1$	$\mathbf{u}^0 = 0$	$\mathbf{u}^0 = 1$	$\mathbf{u}^0 = 0$	$\mathbf{u}^0 = 1$	$\mathbf{u}^0 = 0$
Newton	227	346	35.2	34.0	N/A	N/A
Anderson	35	35	N/A	N/A	5.03	5.06
2-step	20	20	38.4	38.1	5.42	4.5
2-RASPEN	7	6	27.1(8.0)	19.5 (8.5)	5.25	3.85

Table 5: Example 2,  $N = 8 \times 8$  subdomains, results for two different initial guesses  $\mathbf{u}^0 = 0$  and  $\mathbf{u}^0 = 1$ .

Method	Its		GMRES Its (per it)		$N_{it,loc}$	
	$\mathbf{u}^0 = 1$	$\mathbf{u}^0 = 0$	$\mathbf{u}^0 = 1$	$\mathbf{u}^0 = 0$	$\mathbf{u}^0 = 1$	$\mathbf{u}^0 = 0$
Newton	227	346	26.2	25.4	N/A	N/A
Anderson	22	22	N/A	N/A	7.66	7.96
2-step	11	11	30.1	31.9	9.19	9.66
2-RASPEN	7	7	20.4(5.9)	15.3 (6.3)	7.87	6.07

Table 6: Example 2,  $N = 4 \times 4$  subdomains, results for two different initial guesses  $\mathbf{u}^0 = 0$  and  $\mathbf{u}^0 = 1$ .

Method	Its		GMRES Its (per it)		$N_{it,loc}$	
	$\mathbf{u}^0 = 1$	$\mathbf{u}^0 = 0$	$\mathbf{u}^0 = 1$	$\mathbf{u}^0 = 0$	$\mathbf{u}^0 = 1$	$\mathbf{u}^0 = 0$
Newton	227	346	21.0	18.3	N/A	N/A
Anderson	17	17	N/A	N/A	10.0	13.93
2-step	8	8	25.6	25.6	16.19	24.53
2-RASPEN	6	6	15.3(4.3)	13.2 (4.3)	13.33	26.21

Table 7: Example 2,  $N = 2 \times 2$  subdomains, results for two different initial guesses  $\mathbf{u}^0 = 0$  and  $\mathbf{u}^0 = 1$ .

### 6.3. Diffusive Wave Model on Large Realistic Urban Domain

In the final numerical experiment, referred to as Example 3, we consider the Diffusive Wave model (1) used to model a hypothetical flood in a densely urbanized area the city of Nice, France. The model domain is depicted in Figure 7 and has dimension  $850 \times 1500$  meters. In this test case scenario, the flood is produced by an overflow of Paillon river in the north-west part of the domain. Once again, the buildings are removed from the computational domain, leading to a large number of perforations (447 in total). The bathymetry  $z_b$  uses the 1m Digital Elevation Model available from [18]. The parameters of the Diffusive Wave model are chosen formula as  $\alpha = 1.5$  and  $\gamma = 0.5$ , based on Chézy’s formula, with friction coefficient  $c_f = 30$  which corresponding to a rough terrain [29]. We set Dirichlet boundary conditions, with water flow of about 2 metres coming from the Paillon river region and no water flow ( $u = z_b$ ) elsewhere. The initial condition is taken as equal to  $z_b$  and the final simulation time is set to  $T_f = 1500$  seconds, which corresponds to a steady state solution.

Consider the NRAS iteration (16), which contains the solution of local nonlinear subproblems via Newton’s method. In practice, for time-dependent problems, we come across the issue that some local subproblems will not converge for a given time increment  $\Delta t_n = t_{n+1} - t_n$  in the residual function (5). We have found for our numerical examples that often, it is a small portion of subproblems that will not converge, generally due to stagnation in convergence. Therefore, it may be inefficient to reduce the global time increment for all subproblems and the entire iteration. We implement a local time step reduction strategy which makes it possible to reduce the time increment locally, then use this solution as an initial guess for the original system. This process is described in Algorithm 3. In this numerical experiment, with the exception of Newton’s method, the discussed local adaptive time-stepping method of Algorithm 3 is implemented with a global time increment of  $\Delta t = 10$  seconds for each time step for all methods. We find that with this local adaptive time stepping, a global time increment reduction is not necessary for convergence.

For Newton’s method, we begin with an initial time increment of  $\Delta t_0 = 10$  seconds. If the system at a given time step can not be solved, the global time increment will be reduced by a factor of  $\sqrt{2}$  until the reduced system is able to be solved. Then, once the reduced system is solved, we increase the time increment by a factor of  $\sqrt{2}$  for the next time step, with a maximum time increment of 10 seconds. This means that  $\Delta t_{n+1} = \min(\sqrt{2}\Delta t_n, 10)$ . As mentioned, the final time for this experiment is  $T_f = 1500$ .



---

**Procedure 3** Local subproblem with local time-stepping

---

**Require:**  $\Delta t, \mathbf{u}^k$ , initial guess  $G_j^0$ , subdomain index  $j$

Let  $G_j(\mathbf{u}^k; G_j^0; \Delta t)$  denote the solution to the local subproblem (15) with initial guess  $G_j^0$  and time step  $\Delta t$  used in the residual.

$\Delta t_{worked} = \Delta t$

1: Solve local subproblem with some  $\Delta t_{worked} \leq \Delta t$  for  $G_j^w = G_j(\mathbf{u}^k; G_j^0; \Delta t_{worked})$  :

return  $G_j^* = G_j^w$  if  $\Delta t_{worked} = \Delta t$

Initialize  $\Delta t_{try} = \Delta t_{worked}$

**if**  $\Delta t_{worked} < \Delta t$  **then**

  Until convergence:

  2: Use  $G_j^w$  as initial guess for original  $\Delta t$ , try to solve for  $G_j^* = G_j(\mathbf{u}^k; G_j^w; \Delta t)$

**if** Step 2 fails: Initial guess was insufficient to solve original system **then**

    Form better initial guess: Increase  $\Delta t_{try} = \frac{\Delta t + \Delta t_{try}}{2}$  and proceed to step 3

**else** Return  $G_j^*$

**end if**

  3: Obtain new initial guess: Reset and solve for  $G_j^w = G_j(\mathbf{u}^k; G_j^0; \Delta t_{try})$

**if** Step 3 fails: Solve didn't converge for  $\Delta t_{try}$  **then**

    Reduce  $\Delta t_{try} = \frac{\Delta t_{worked} + \Delta t_{try}}{2}$  and return to step 3

**else** Solve converged for  $\Delta t_{try}$  and new initial guess  $G_j^w$  obtained

    Set  $\Delta t_{worked} = \Delta t_{try}$  and return to step 2

**end if**

**end if**

---

Figure 7 reports the simulation results for time  $t = 10, 250, 500$ , and  $1500$  seconds. In particular, in color, we report the water depth  $\mathbf{h} = \mathbf{u} - z_b(\mathbf{x})$  over the “flooded region” where  $\mathbf{h} \geq 1\text{cm}$ . The ground surface elevation  $z_b$  is reported in black and white.

The spatial discretization results in 81444 mesh points and 131581 triangles in the model domain. As mentioned, the fine-scale triangulation will be conforming to the polygonal coarse partitioning. Although we record results for various numbers of subdomains  $N$ , the fine-scale mesh will be kept consistent throughout the experiment and is conforming to a  $N = 8 \times 16$  coarse mesh; therefore, it will conforming to  $N = 1 \times 2$ ,  $N = 2 \times 4$ ,  $N = 4 \times 8$  meshes as well. The coarse and fine partitionings are shown in Figure 6 for multiple coarse partitionings. By the end of the simulation, 38216 points and 60846 triangles are “flooded” such that  $h \geq 1\text{cm}$ . The total number of coarse nodes are given by  $N_V = 795, 357, 126$ , and  $34$  for  $N = 8 \times 16, 4 \times 8, 2 \times 4$ , and  $1 \times 2$  subdomains, respectively. The overlap is once again set to  $\frac{1}{20}\mathcal{H}_j$ .

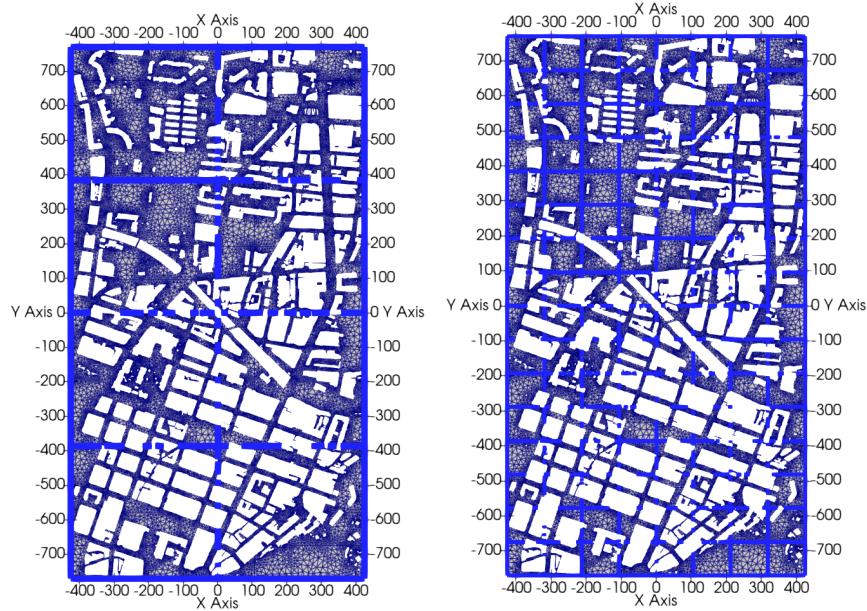


Figure 6: Coarse (thick blue lines) and fine (thin blue lines) discretization for  $N = 2 \times 4$  (left) and  $N = 8 \times 16$  (right) subdomains for model domain representing the Nice port and Paillon river.

Recall that at every time step, the nonlinear system (5) has to be solved. For this example, in addition to Newton’s method given by Algorithm 1, we provide numerical results for the two-step method from Algorithm 4, the one-level RASPEN method from Algorithm 2, the two-level RASPEN method from Algorithm 3, and the Anderson acceleration method from Algorithm 5.

Figure 8 displays the cumulative number of (successful) outer iterations over the simulation time, obtained for each of the methods for various numbers of subdomains  $N$ . In addition, Tables 8, 9, 10 and 11 report the total number of outer iterations and the number of successful time steps. In addition, whenever appropriate, Tables 8, 9, 10 and 11 reports the number of GMRES and NRAS iterations. Instead of GMRES iterations per outer iter-

ation, we display the cumulative number of GMRES iterations summed over all time steps and all outer iterations. For the two-step and Newton methods, at each outer iteration, the linear system is solved using GMRES method combined with the linear two-level RAS preconditioner (14). The number of GMRES iterations per outer iteration averaged over each time step are reported at Figure 9. The overall (cumulative) number of GMRES iterations is reported in Tables 8, 9, 10, and 11 for  $N = 8 \times 16, 4 \times 8, 2 \times 4, 1 \times 2$ , respectively.

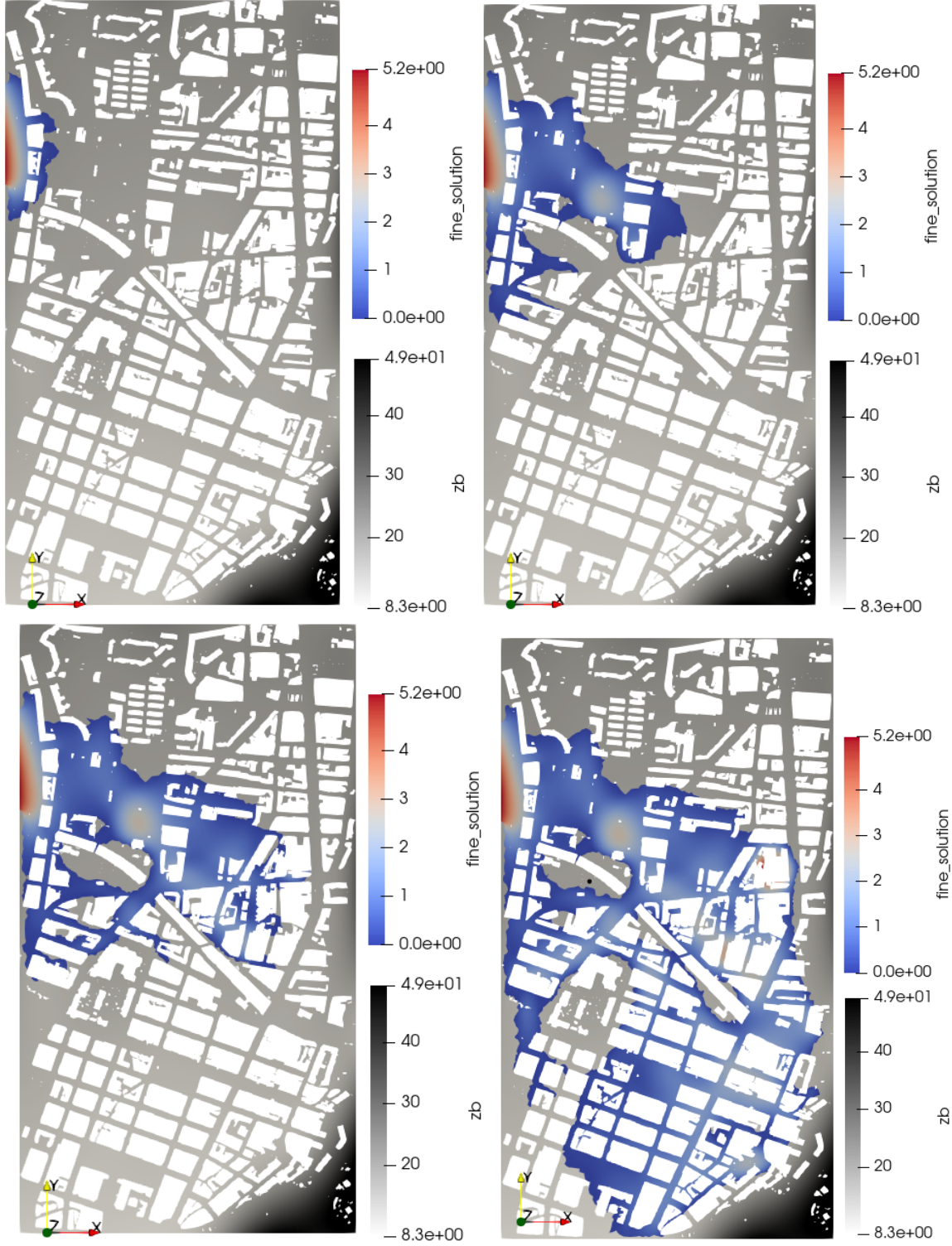


Figure 7: Numerical solution of Example 3 at various time steps, where the numerical solution is presented by  $\mathbf{h} = \mathbf{u} - z_b(\mathbf{x})$ . Top:  $t = 10$  (left) seconds,  $t = 250$  (right) seconds. Bottom:  $t = 500$  (left) seconds, final  $t = 1500$  (right) seconds. “Flooded” region (where  $\mathbf{h} \geq 1\text{cm}$ ) are shown in colour, with underlying bathymetry  $z_b$  shown in the background in black and white.

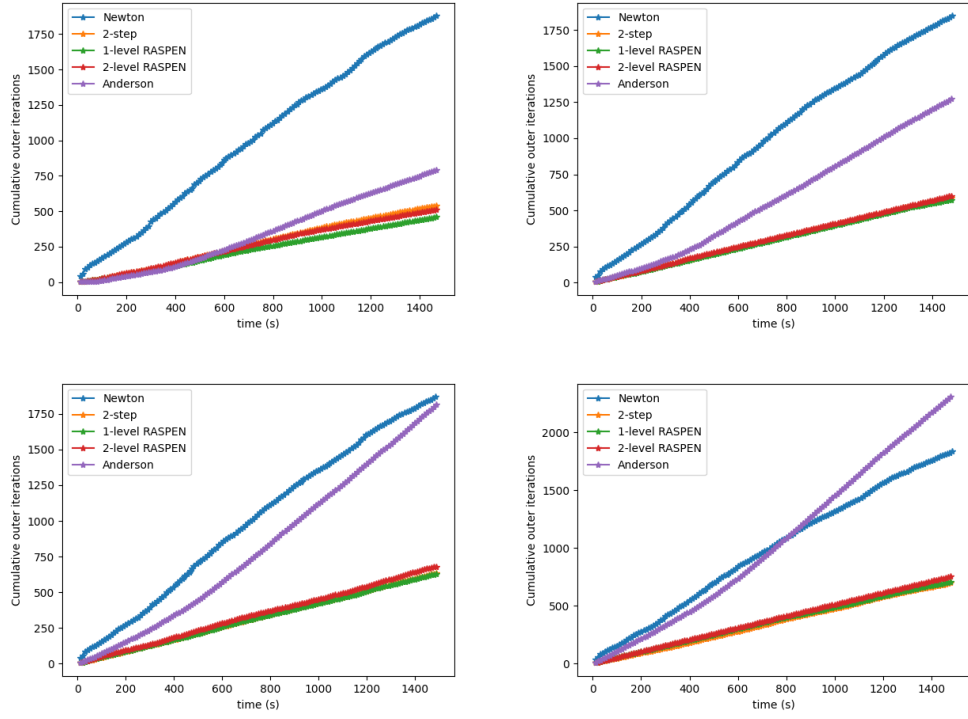


Figure 8: Example 3, cumulative outer iterations. Top:  $N = 1 \times 2$  (left),  $N = 2 \times 4$  (right). Bottom:  $N = 4 \times 8$  (left),  $N = 8 \times 16$  (right).

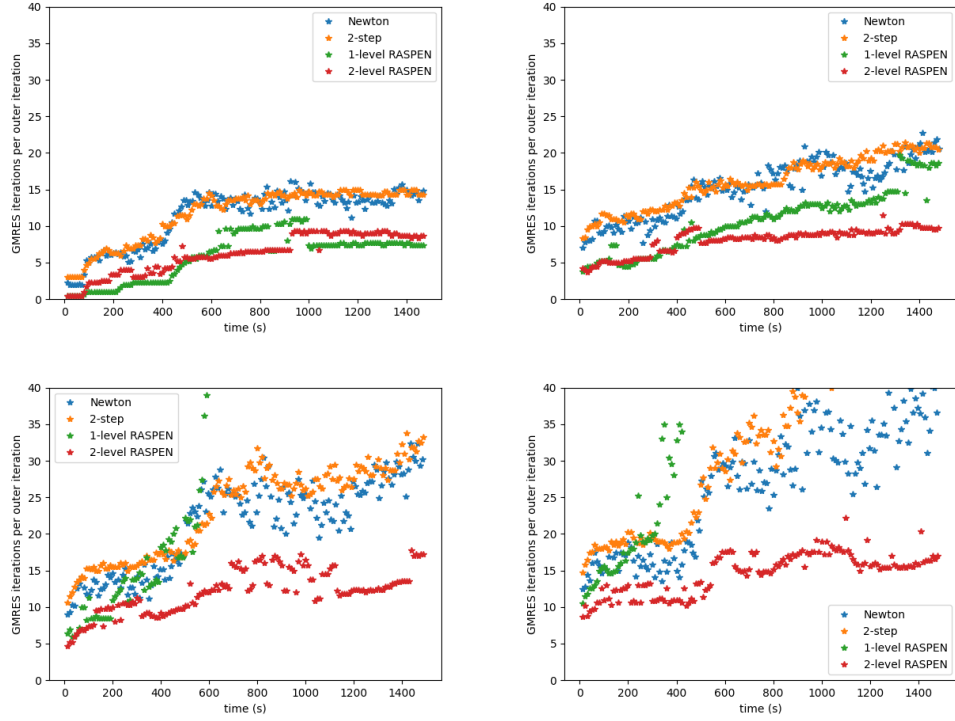


Figure 9: Example 3, GMRES iterations at each global outer iteration over time. Top:  $N = 1 \times 2$  (left),  $N = 2 \times 4$  (right). Bottom:  $N = 4 \times 8$  (left),  $N = 8 \times 16$  (right).

Method	T. steps	Outer Its	GMRES Its	$N_{it,loc}$
Newton	155	1797	44146	N/A
Anderson	150	2524	N/A	1.81
2-step	150	687	20029	1.51
1-level RASPEN	150	686	100453	1.53
2-level RASPEN	150	730	12117(+2907 coarse)	1.84

Table 8: Example 3,  $N = 8 \times 16$  subdomains.

Method	T. steps	Outer Its	GMRES Its	$N_{it,loc}$
Newton	160	1807	33432	N/A
Anderson	150	1902	N/A	2.44
2-step	150	638	13164	1.91
1-level RASPEN	150	624	33117	1.95
2-level RASPEN	150	650	8065(+2031 coarse)	2.39

Table 9: Example 3,  $N = 4 \times 8$  subdomains.

Method	T. steps	Outer Its	GMRES Its	$N_{it,loc}$
Newton	151	1776	26753	N/A
Anderson	150	1657	N/A	3.43
2-step	150	592	9483	2.72
1-level RASPEN	150	571	9040	2.89
2-level RASPEN	150	595	6328(+1755 coarse)	3.44

Table 10: Example 3,  $N = 2 \times 4$  subdomains.

Method	T. steps	Outer Its	GMRES Its	$N_{it,loc}$
Newton	155	1791	21608	N/A
Anderson	150	1225	N/A	3.89
2-step	150	597	7794	4.28
1-level RASPEN	150	477	3827	4.72
2-level RASPEN	150	515	3983(+1114 coarse)	4.79

Table 11: Example 3,  $N = 1 \times 2$ .

From Figure 8, we see that the RASPEN variants (both 1 and two-level) as well as the two-step method produce the smallest number of outer iterations, and are very similar to one another in this regard. Additionally, we see that the Anderson acceleration changes the most as we increase  $N$ , with the outer iterations generally increasing. As expected, Newton's method results in a higher number of outer iterations when compared to the RASPEN and two-step methods.

We see from Figure 9 that as the number of subdomains is increased, the one-level RASPEN method is no longer scalable; in fact, the GMRES solves per iteration are significantly larger than the other methods such that they are out of the scope of the vertical axis in the figure (green dots in Figure 9). Additionally, as the number of subdomains grow, two-level RASPEN clearly becomes the method which contains the lowest average number of GMRES iterations per outer iteration. As far as Newton’s method preconditioned with the two-level linear RAS preconditioner (blue dots in Figure 9), the method is fairly scalable, as the number of GMRES iterations are not increasing proportionally with  $N$ . However, we do see a slight increase as the number of subdomains is increased. We remark additionally that the Two-step method produces very similar results when compared to the preconditioned Newton’s method, as the Two-step method also involves a linearly preconditioned system via the two-level linear RAS preconditioner.

From Table 8, 9, 10, and 11, we see the results from Figures 8 and 9 summarized. Particularly, Newton’s method results in much larger numbers of outer iterations when compared to the nonlinearly preconditioned variants (with the exception of the Anderson acceleration as  $N$  grows large). Additionally, the GMRES iterations in one-level RASPEN grow as  $N$  grows. It appears that if as the number of subdomains grows, two-level RASPEN is the most efficient, produces the lowest number of GMRES iterations with a relatively small number of coarse linear solves. We remark again that the coarse linear solves are computationally less expensive a global fine-scale linear solve.

Overall, from our numerical experiments, we draw the following conclusions. As expected, one-level RASPEN is not a scalable method as the number of subdomains  $N$  grows large; for this reason, we do not generally recommend its use. For a stationary problem, Newton’s method is much more sensitive to the initial guess than the other proposed methods, with iteration counts increasing by up to 50%. While Newton’s method preconditioned with the two-level RAS method produces a fairly scalable iteration, the addition of an NRAS solve in the two-step method greatly accelerates the convergence. Additionally, the two-step method is quite straightforward to implement, and in principle the global linear system can be done via a direct solve (provided the system is not too large). For this linearized system in the Two-step and Newton’s methods, the Trefftz space performs well as a component of the two-level RAS preconditioner. However, when implemented, the two-level RASPEN method further reduces the total number of GMRES iterations compared to the Two-step and Newton methods. Additionally, specifically for the porous media examples, the two-level RASPEN method provides a significant acceleration in terms of outer iterations. The Anderson acceleration of a coarse two-step method is also an interesting alternative to Newton’s method, reducing the total iteration count. However, we do not generally recommend it over the two-step and two-level RASPEN methods.

## 7. Summary and Future Work

This article has provided a numerical experiment of multiple nonlinear domain decomposition methods to solve nonlinear equations on perforated domains. Specifically, we have focused on a Diffusive Wave model on a domain with a large number of perforations; these



perforations represent buildings and fall/fences in urban areas. We have found that nonlinear preconditioning techniques, particularly two-level RASPEN with the coarse space from [4], greatly reduce the number of outer iterations for both tested model problems. Not only are the number of outer iterations reduced when compared to Newton’s method, but the inner number of GMRES iterations per outer iteration are reduced as well. Additionally, the two-step method which adds a nonlinear RAS iteration to each Newton iteration, is straightforward to implement and greatly reduces the number of outer and GMRES iterations; in principle, the sparse large linear system in the Two-step method could be solved via a direct solve. Furthermore, we have found that local time step reduction is an efficient method to eliminate the need for a global time step reduction for all subdomains. Future work involves load-balancing of the complexity of the subdomains and parallel implementation to provide detailed runtimes.

## References

- [1] M. ABILY, N. BERTRAND, O. DELESTRE, P. GOURBESVILLE, AND C.-M. DULUC, *Spatial global sensitivity analysis of high resolution classified topographic data use in 2d urban flood modelling*, Environmental Modelling & Software, 77 (2016), pp. 183–195.
- [2] R. ALONSO, M. SANTILLANA, AND C. DAWSON, *On the diffusive wave approximation of the shallow water equations*, Eur. J. Appl. Math., 19 (2008), pp. 575–606.
- [3] L. ANDRES, *L’apport de la donnée topographique pour la modélisation 3D fine et classifiée d’un territoire*, Rev. XYZ, 133 (2012), pp. 24–30.
- [4] M. BOUTILIER, K. BRENNER, AND V. DOLEAN, *Robust methods for multiscale coarse approximations of diffusion models in perforated domains*, arXiv preprint arXiv:2310.15669, (2023).
- [5] K. BRENNER, *On global and monotone convergence of the preconditioned newton’s method for some mildly nonlinear systems*, in International Conference on Domain Decomposition Methods, Springer, 2022, pp. 85–92.
- [6] X.-C. CAI, W. D. GROPP, D. E. KEYES, AND M. D. TIDRIRI, *Newton-krylov-schwarz methods in cfd*, in Numerical methods for the Navier-Stokes equations: Proceedings of the International Workshop Held at Heidelberg, October 25–28, 1993, Springer, 1994, pp. 17–30.
- [7] X.-C. CAI AND D. E. KEYES, *Nonlinearly preconditioned inexact newton algorithms*, SIAM Journal on Scientific Computing, 24 (2002), pp. 183–200.
- [8] X.-C. CAI AND X. LI, *Inexact newton methods with restricted additive schwarz based nonlinear elimination for problems with high local nonlinearity*, Siam journal on scientific computing, 33 (2011), pp. 746–762.

- [9] —, *Inexact newton methods with restricted additive schwarz based nonlinear elimination for problems with high local nonlinearity*, Siam journal on scientific computing, 33 (2011), pp. 746–762.
- [10] F. CHAOUQUI, M. J. GANDER, P. M. KUMBHAR, AND T. VANZAN, *Linear and non-linear substructured restricted additive schwarz iterations and preconditioning*, Numerical Algorithms, 91 (2022), pp. 81–107.
- [11] —, *On the nonlinear dirichlet–neumann method and preconditioner for newton’s method*, in Domain Decomposition Methods in Science and Engineering XXVI, Springer, 2023, pp. 381–389.
- [12] P. G. CIARLET, *The finite element method for elliptic problems*, SIAM, 2002.
- [13] V. DOLEAN, M. J. GANDER, W. KHERIJI, F. KWOK, AND R. MASSON, *Nonlinear preconditioning: How to use a nonlinear schwarz method to precondition newton’s method*, SIAM Journal on Scientific Computing, 38 (2016), pp. A3357–A3380.
- [14] C. EVANS, S. POLLOCK, L. G. REBHOLZ, AND M. XIAO, *A proof that anderson acceleration improves the convergence rate in linearly converging fixed-point methods (but not in those converging quadratically)*, SIAM Journal on Numerical Analysis, 58 (2020), pp. 788–810.
- [15] A. HEINLEIN AND M. LANSER, *Additive and hybrid nonlinear two-level schwarz methods and energy minimizing coarse spaces for unstructured grids*, SIAM Journal on Scientific Computing, 42 (2020), pp. A2461–A2488.
- [16] A. J. HOFFMAN, M. S. MARTIN, AND D. J. ROSE, *Complexity bounds for regular finite difference and finite element grids*, SIAM Journal on Numerical Analysis, 10 (1973), pp. 364–369.
- [17] F.-N. HWANG AND X.-C. CAI, *A class of parallel two-level nonlinear schwarz preconditioned inexact newton algorithms*, Computer methods in applied mechanics and engineering, 196 (2007), pp. 1603–1611.
- [18] INSTITUT NATIONAL DE L’INFORMATION GÉOGRAPHIQUE ET FORESTIÈRE (IGN), *RGE ALTI® - Digital Terrain Model*, 2024. <https://geoservices.ign.fr/rgealti>.
- [19] C. KAMTHORNCHAROEN, *Two-level Restricted Additive Schwarz Preconditioned Exact Newton with Applications*, PhD thesis, 2022.
- [20] A. KLAWONN, M. LANSER, AND O. RHEINBACH, *Nonlinear feti-dp and bddc methods*, SIAM Journal on Scientific Computing, 36 (2014), pp. A737–A765.
- [21] A. KLAWONN, M. LANSER, AND O. RHEINBACH, *Nonlinear bddc methods with approximate solvers*, Electronic Transactions on Numerical Analysis, 49 (2018), pp. 244–273.

- [22] A. Klawonn, M. Lanser, and O. Rheinbach, *Nonlinear bddc methods with approximate solvers*, (2018).
- [23] A. Klawonn, M. Lanser, O. Rheinbach, and M. Ulan, *Nonlinear feti-dp and bddc methods: A unified framework and parallel results*, SIAM Journal on Scientific Computing, 39 (2017), pp. C417–C451.
- [24] L. Liu and D. E. Keyes, *Field-split preconditioned inexact newton algorithms*, SIAM Journal on Scientific Computing, 37 (2015), pp. A1388–A1409.
- [25] L. Liu, D. E. Keyes, and R. Krause, *A note on adaptive nonlinear preconditioning techniques*, SIAM Journal on Scientific Computing, 40 (2018), pp. A1171–A1186.
- [26] C. Negrello, P. Gosselet, and C. Rey, *Nonlinearly preconditioned feti solver for substructured formulations of nonlinear problems*, Mathematics, 9 (2021), p. 3165.
- [27] J. R. Shewchuk, *Triangle: Engineering a 2d quality mesh generator and delaunay triangulator*, in Workshop on applied computational geometry, Springer, 1996, pp. 203–222.
- [28] H. F. Walker and P. Ni, *Anderson acceleration for fixed-point iterations*, SIAM Journal on Numerical Analysis, 49 (2011), pp. 1715–1735.
- [29] F. M. White, C. Ng, and S. Saimek, *Fluid mechanics*, McGraw-Hill, cop., 2011.
- [30] D. Yu and S. N. Lane, *Urban fluvial flood modelling using a two-dimensional diffusion-wave treatment, part 1: mesh resolution effects*, Hydrological Processes: An International Journal, 20 (2006), pp. 1541–1565.
- [31] —, *Urban fluvial flood modelling using a two-dimensional diffusion-wave treatment, part 2: development of a sub-grid-scale treatment*, Hydrological Processes: An International Journal, 20 (2006), pp. 1567–1583.